

# Viscoelastic Flows with Complex Free Surfaces : Numerical Analysis and Simulation

Andrea Bonito <sup>1</sup>

Department of Mathematics  
Texas A&M University  
College Station, TX 77843, USA

Philippe Clément

Analysis Group  
TU Delft  
Mekelweg 4, 2628 CD Delft, The Netherlands

Marco Picasso

Institut d'Analyse et Calcul Scientifique  
Ecole Polytechnique Fédérale de Lausanne  
1015 Lausanne, Switzerland

November 8, 2009

<sup>1</sup>Partially supported by the Swiss National Science Foundation and NSF Grant DMS-0914977.



# Contents

<b>1 Modelling</b>	<b>5</b>
1.1 Macroscopic Models . . . . .	8
1.1.1 Differential Models . . . . .	8
1.1.2 Integral Models . . . . .	9
1.2 Mesoscopic Models . . . . .	10
1.2.1 The Dumbbells Model . . . . .	11
1.2.2 Link Between Hookean Dumbbells and the Oldroyd-B Model	14
1.3 Initial and Boundary Conditions . . . . .	15
1.4 Summary . . . . .	17
<b>2 Numerical Analysis of Simplified Problems</b>	<b>19</b>
2.1 Numerical models for viscoelastic flows . . . . .	19
2.1.1 Numerical Computations . . . . .	19
2.1.2 Mathematical Analysis . . . . .	22
2.1.3 Numerical Analysis . . . . .	24
2.2 Time Discretization : an Operator Splitting Scheme . . . . .	28
2.2.1 The Free Surface Oldroyd-B Model . . . . .	28
2.2.2 The Free Surface FENE Dumbbells Model . . . . .	30
2.3 The Three Fields Stokes Problem . . . . .	31
2.3.1 The Continuous Problem . . . . .	31
2.3.2 Finite Element Discretizations . . . . .	33
2.4 A Simplified Oldroyd-B Problem . . . . .	36
2.5 A Simplified Hookean Dumbbells Problem . . . . .	39
<b>3 Numerical simulation</b>	<b>45</b>
3.1 Space Discretization : Structured Cells and Finite Elements . . . . .	45
3.1.1 Advection Step : Structured Grid of Cubic Cells . . . . .	46
3.1.2 Correction Step : Stokes and Oldroyd-B with Finite Elements . . . . .	52
3.1.3 Implementations Details . . . . .	54
3.2 Extension to Mesoscopic Models . . . . .	54
3.3 Numerical Results . . . . .	55
3.3.1 Numerical Validation . . . . .	55
3.3.2 Jet Buckling . . . . .	59

3.3.3 Filament Stretching . . . . .	60
-------------------------------------	----

# Chapter 1

## Modelling of Viscoelastic Flows with Complex Free Surfaces

Viscoelastic flows with complex free surfaces are considered. Such flows are involved in several industrial processes involving paints, plastics, food or adhesives but also in geophysical applications such as mud flows or avalanches.

Viscoelastic fluids are viscous fluids having elastic properties. They cannot be described with the classical theories of fluid or continuum mechanics. Additional laws have to be added in order to relate the stress to the velocity, this being the scope of rheology.

The rheology of viscoelastic flows depends on the microscopic details of the fluid. As a consequence, an accurate mathematical modelling should consider all the physical scales involved. Consider for instance the case of a polymeric liquid, say polyethylene  $(C_2H_4)_n$ , where  $n = 10^4$  is the number of monomers. Since the size of the  $C - C$  bond is  $10^{-10} m$ , then the size of the fully extended molecule is  $10^{-10} \times 10^4 = 10^{-6} m$ , whereas the size of the macroscopic workpiece - a car bumper for instance - is about  $1 m$ . Clearly, all these microscopic details cannot be included in a macroscopic numerical simulation but intermediate - mesoscopic - models can be considered. Only the simplest macroscopic and mesoscopic models are considered here. More realistic and complex models can be found in classical textbooks of non-Newtonian flows, see [13, 82, 113, 125] for instance. We also refer to [137] for the description of suspended particles in a viscoelastic flow.

Consider a cavity  $\Lambda$  of  $\mathbb{R}^d$ ,  $d = 2$  or  $3$ , partially filled with a viscoelastic fluid. We are interested in computing the fluid shape between time  $0$  and time  $T$ . The notations are reported in Fig. 1.1 and are the following. Let  $D(t) \subset \Lambda$  be the liquid region at time  $t$  and let  $\varphi : \Lambda \times (0, T)$  be the characteristic function

of the liquid, that is

$$\begin{aligned}\varphi(x, t) &= 1 && \text{if } x \in D(t), \\ &= 0 && \text{if not.}\end{aligned}$$

Then, the space-time domain  $D_T$  containing the fluid is defined by

$$D_T = \{(x, t) \in \Lambda \times (0, T); \varphi(x, t) = 1\}. \quad (1.1)$$

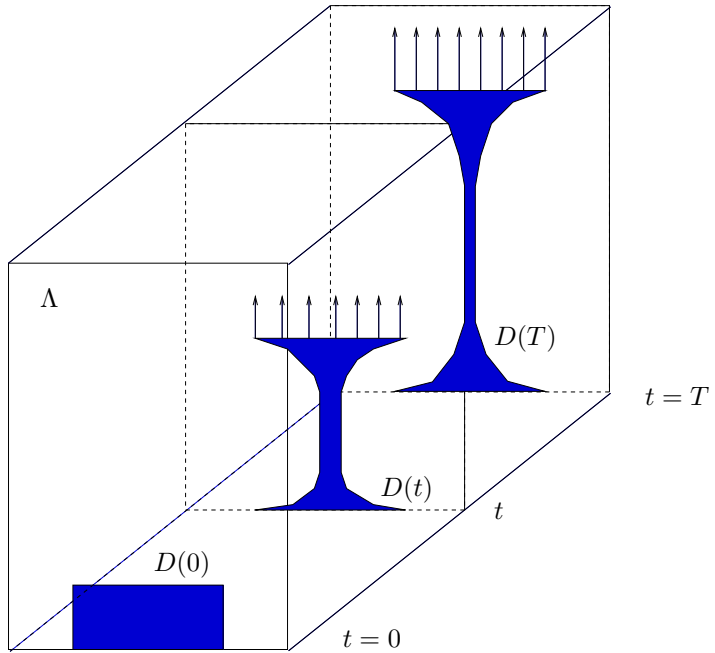


Figure 1.1: Notations. The stretching of a filament in two space dimensions is considered. At initial time, the viscoelastic fluid is at rest and occupies the domain  $D(0)$ , which is part of the cavity  $\Lambda$ . At  $t > 0$ , the upper part of the liquid domain moves at given velocity, the fluid domain is  $D(t)$ .

In the liquid region  $D_T$ , the momentum equation writes

$$\rho \frac{\partial u}{\partial t} + \rho(u \cdot \nabla)u - \operatorname{div} \sigma^{tot} = f. \quad (1.2)$$

Here  $\rho$  is the fluid density,  $u : D_T \rightarrow \mathbb{R}^d$  the fluid velocity,  $\sigma^{tot} : D_T \rightarrow \mathbb{R}^{d \times d}$  the total stress tensor of the fluid and  $f : D_T \rightarrow \mathbb{R}^d$  are volume forces, for instance gravity forces  $f = \rho g$ . Consider the case of a polymeric fluid, that is a Newtonian solvent plus polymer chains. Then, the total stress is the sum of a Newtonian contribution and a non-Newtonian one

$$\sigma^{tot} = 2\eta_s \epsilon(u) - pI + \sigma, \quad (1.3)$$

where  $\eta_s \geq 0$  is the solvent viscosity,  $\epsilon(u) = \frac{1}{2}(\nabla u + \nabla u^T)$  is the symmetric part of the velocity gradient with  $(\nabla u)_{ij} = \partial u_i / \partial x_j$ ,  $p : D_T \rightarrow \mathbb{R}$  denotes the pressure,  $I$  the unit tensor in  $\mathbb{R}^{d \times d}$  and  $\sigma$  the extra-stress (the non-Newtonian part of the stress) due to the polymer chains for instance. Inserting (1.3) into (1.2) and assuming incompressibility yields the following mass and momentum equations

$$\rho \frac{\partial u}{\partial t} + \rho(u \cdot \nabla)u - 2\eta_s \operatorname{div} \epsilon(u) + \nabla p - \operatorname{div} \sigma = f, \quad (1.4)$$

$$\operatorname{div} u = 0, \quad (1.5)$$

in the liquid domain  $D_T$ .

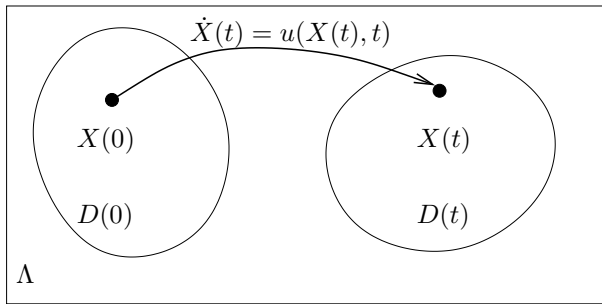


Figure 1.2: Trajectories of a fluid particle from time 0 to time  $t$ . The liquid domain at time  $t$  is  $D(t)$ , the cavity containing the liquid is  $\Lambda$ .

In order to obtain the space-time liquid domain  $D_T$  defined by (1.1), Lagrangian or Eulerian methods can be advocated. Since our aim is to solve flows in complex domains such as jet buckling or fingering instabilities, we shall consider Eulerian methods so that an equation is needed for the characteristic function  $\varphi$  of the liquid region. Again, we have the choice between level set [136, 112] methods or Volume of Fluid (VOF) [127, 134] methods. We select here the VOF formulation and obtain this equation by assuming that all the fluid particles move with the fluid velocity  $u$ . Therefore, given the liquid domain  $D(0)$  at time 0, the liquid domain at time  $t$  is given by

$$D(t) = \{X(t) \in \Lambda \text{ such that } \dot{X}(t) = u(X(t), t) \text{ with } X(0) \in D(0)\}, \quad (1.6)$$

see Fig. 1.2. Hereabove, it is understood that the velocity  $u$  is smooth enough so that the differential equation  $\dot{X}(t) = u(X(t), t)$  has a unique solution, for instance  $u$  continuous and Lipschitz with respect to the space variable. We now claim that if the function  $\varphi$  satisfies

$$\frac{\partial \varphi}{\partial t} + u \cdot \nabla \varphi = 0 \quad \text{in } \Lambda \times (0, T), \quad (1.7)$$

in a weak sense and if  $\varphi(\cdot, 0)$  is the characteristic function of  $D(0)$ , then  $\varphi(\cdot, t)$  is the characteristic function of  $D(t)$ . Indeed, the solution of (1.7) is given by

$$\varphi(X(t), t) = \varphi(X(0), 0), \quad \text{where } \dot{X}(t) = u(X(t), t), \quad 0 \leq t \leq T.$$

Since  $\varphi(\cdot, 0)$  is the characteristic function of  $D(0)$ , we therefore have

$$\varphi(X(t), t) = \varphi(X(0), 0) = 1 \quad \text{for all } X(0) \in D(0).$$

Using (1.6) we finally obtain

$$\varphi(X(t), t) = 1 \quad \text{for all } X(t) \in D(t),$$

thus  $\varphi(\cdot, t)$  is the characteristic function of  $D(t)$ .

Let us summarize the situation. Our goal is to find the characteristic function of the liquid  $\varphi$  in the whole cavity  $\Lambda$ , the velocity  $u$ , pressure  $p$  and extra-stress  $\sigma$  in the liquid region  $D(t)$  and satisfying (1.4), (1.5) and (1.7). We still need to provide a relation between  $u$  and  $\sigma$ . This can be done by considering either macroscopic or mesoscopic models.

## 1.1 Macroscopic Models

When considering viscoelastic flows at macroscopic scale, one has to choose between differential and integral models. In chap. 3, numerical results will be presented when considering the simplest of the differential models presented here, namely the Oldroyd-B model. However, a brief presentation of differential and integral models is proposed hereafter. We refer again to [13, 82, 113, 125] for classical textbooks and to the contribution of Lozinski and Phillips in this book.

### 1.1.1 Differential Models

The simplest differential model is the so-called Oldroyd-B constitutive equation

$$\sigma + \lambda \left( \frac{\partial \sigma}{\partial t} + u \cdot \nabla \sigma - \nabla u \sigma - \sigma \nabla u^T \right) = 2\eta_p \epsilon(u), \quad (1.8)$$

where  $\lambda \geq 0$  is the fluid relaxation time,  $\eta_p \geq 0$  the polymer viscosity. The term  $\nabla u \sigma$  denotes the matrix-matrix product between  $\nabla u$  and  $\sigma$  and the expression within the parenthesis is the upper convected derivative of  $\sigma$ . When the solvent viscosity  $\eta_s$  vanishes, (1.4), (1.5) and (1.8) is the upper convected Maxwell model. Many other models are available in the literature [13, 82], for instance the extra-stress of the eight modes Oldroyd-B model is defined by  $\sigma = \sigma_1 + \dots + \sigma_8$ , where each  $\sigma_i$ ,  $i = 1, 8$ , satisfies (1.8) with  $\lambda$  replaced by the  $i$ -th relaxation time  $\lambda_i$ . Also, the corotational Oldroyd-B model is obtained by replacing the terms  $-\nabla u \sigma - \sigma \nabla u^T$  in (1.8) by

$$\frac{1}{2} \left( \sigma (\nabla u - \nabla u^T) - (\nabla u - \nabla u^T) \sigma \right).$$

The Oldroyd-B model can be generalized to models involving more derivatives, for instance the third order retarded motion model, see [13] for instance. Finally, nonlinear extensions of the Oldroyd-B model have been proposed, for instance the Giesekus, Leonov and Phan-Thien Tanner models are contained in the general formulation

$$f(\sigma)\sigma + \lambda \left( \frac{\partial \sigma}{\partial t} + u \cdot \nabla \sigma - \nabla u \sigma - \sigma \nabla u^T \right) = 2\eta_p \epsilon(u),$$

where  $f(\sigma)$  is a scalar function depending on  $\sigma$  and  $tr(\sigma)$ . Constitutive equations can be specialized to particular viscoelastic fluids. For instance, the Rolie-Poly model is designed for entangled polymer melts [92], the Extended Pom-Pom model [142] has been developed in order to take into account the morphology of branched polymer melts.

Although the Oldroyd-B model (1.8) is too simple to reproduce some of the viscoelastic effects reported in experiments - shear thinning in shear flows for instance - it already contains mathematical difficulties absent in Newtonian flows. Moreover, as we will see in sect. 1.2, this model is linked to the simplest mesoscopic model, namely the Hookean dumbbells model.

### 1.1.2 Integral Models

Following [94], the integral (Lagrangian) formulation of the Oldroyd-B model (1.8) is the following. Let  $x \in D(0)$  be the initial position of a particle moving with the fluid velocity  $u$ . The position of this particle at time  $t$  is denoted by  $X(t)$  and is the solution at time  $t$  of

$$\begin{aligned} \dot{X}(s) &= u(X(s), s) & 0 \leq s \leq t, \\ X(0) &= x, \end{aligned}$$

or equivalently

$$X(t) = x + \int_0^t u(X(s), s) ds. \quad (1.9)$$

Let  $F : D(0) \times (0, T) \rightarrow \mathbb{R}^{d \times d}$  be the deformation tensor defined by

$$F(x, t) = \frac{\partial X}{\partial x}(t) \quad x \in D(0), \quad t \geq 0.$$

Then, the integral formulation of the extra-stress for an Oldroyd-B fluid writes, in Lagrangian coordinates :

$$\begin{aligned} \tilde{\sigma}(x, t) &= \frac{\eta_p}{\lambda^2} \left( \int_0^t e^{-(t-s)/\lambda} F(x, t) F^{-1}(x, s) F^{-T}(x, s) F^T(x, t) ds \right. \\ &\quad \left. + \lambda(F(x, t) F^T(x, t) - I) \right), \quad (1.10) \end{aligned}$$

for all  $x \in D(0)$  and  $t \geq 0$ . We now check that (1.10) indeed coincides with the Oldroyd-B model (1.8). Differentiating (1.9) with respect to  $x$  and  $t$  yields

$$\frac{\partial F}{\partial t}(x, t) = \nabla u(X(t), t)F(x, t) \quad x \in D(0), \quad t \geq 0,$$

so that  $\tilde{\sigma}$  defined by (1.10) satisfies

$$\begin{aligned} \frac{\partial \tilde{\sigma}}{\partial t}(x, t) + \frac{1}{\lambda} \tilde{\sigma}(x, t) &= \nabla u(X(t), t)\tilde{\sigma}(x, t) + \tilde{\sigma}(x, t)\nabla u(X(t), t)^T \\ &\quad + \frac{\eta_p}{\lambda} (\nabla u(X(t), t) + \nabla u(X(t), t)^T). \end{aligned}$$

Finally, we introduce the extra-stress in Eulerian coordinates  $\sigma : D_T \rightarrow \mathbb{R}^{d \times d}$  defined by :

$$\sigma(X(t), t) = \tilde{\sigma}(x, t) \quad x \in D(0), \quad t \geq 0,$$

and check that  $\sigma$  satisfies (1.8).

Several extensions of the integral Oldroyd-B model have been proposed, for instance the famous K-BKZ model, see [13] sect. 8.3. Implementing integral models in complex flows requires some additional effort, see for instance [75] for a review. Indeed, the particles path has to be stored - at least during some time proportional to the relaxation time  $\lambda$  - which is expensive to implement. Therefore, integral formulations will not be considered in this contribution.

## 1.2 Mesoscopic Models

Consider a polymeric liquid that is a newtonian solvent and polymer chains. Polymers chains are long molecules made out of many identical blocks called monomers. The modelling of liquid polymers ranges from the atomic to the mesoscopic scale.

At the atomic scale, molecular dynamics can be considered in order to study specific problems such as single chains in a flow, rupture of a filament or nanodrops. For instance in [79], a polymer melt is considered. A FENE (Finitely Extensible Nonlinear Elastic) potential applies between two monomers of a given chain, whereas a Lennard-Jones potential acts between two monomers not belonging to the same chain. Such simulations are of interest in localized regions but cannot be performed at the macroscopic level. Another possibility is to consider a kinetic theory of liquid polymers.

At the mesoscopic level, polymer chains can be modelled by a collection of beads connected with springs, the Rouse chain, see Fig. 1.3. When considering a dilute solution of polymers (a spaghetti soup), the chains do not interact each other, the interaction is only through the Newtonian solvent. When considering a polymer melt (a plate of spaghetti), the chains are entangled and the movement of the beads is possible only along the chain : the chains reptates. From the industrial viewpoint, most processes involve polymer melts rather than dilute solutions. However, dilute solutions are better understood from the

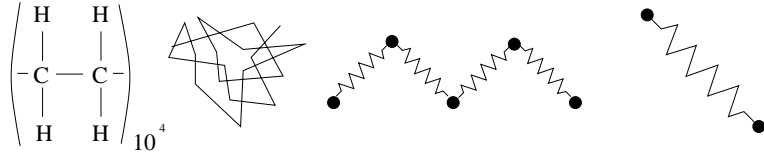


Figure 1.3: Modelling of polymer chains from nanoscale to mesoscale. From left to right : polyethylene, polymer chain, the Rouse chain, a dumbbell.

mathematical viewpoint and we will focus in this contribution on dilute solutions. Moreover, we will even simplify the Rouse chain model and consider the dumbbells model, that is two beads connected with an elastic spring, see again Fig. 1.3. Due to the increase of computer power, realistic numerical simulations can be nowadays performed on chains, see [76] and the references therein.

### 1.2.1 The Dumbbells Model

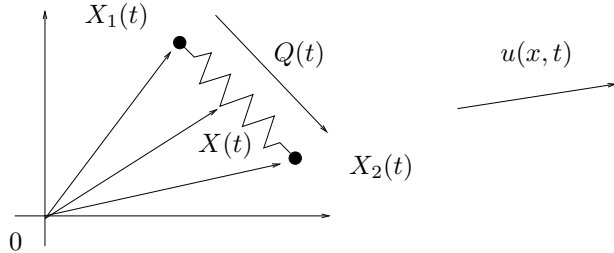


Figure 1.4: A dumbbell placed in a flow field  $u(x, t)$ . The beads positions are  $X_1(t)$  and  $X_2(t)$ , the spring elongation is  $Q(t) = X_2(t) - X_1(t)$ , the center of mass is  $X(t) = \frac{1}{2}(X_1(t) + X_2(t))$ .

Consider as in Fig. 1.4 a dumbbell. The two beads positions are denoted by  $X_1(t)$ ,  $X_2(t)$ , the spring elongation is  $Q(t) = X_2(t) - X_1(t)$ , the center of mass is  $X(t) = \frac{1}{2}(X_1(t) + X_2(t))$ . We now derive a stochastic differential equation for the elongation  $Q(t)$ . The forces acting on each bead are i) the drag force which is proportional to the relative velocity  $\dot{X}_i(t) - u(X_i(t), t)$  between the velocity of bead  $i$  and the fluid velocity,  $i = 1, 2$  ii) the elastic force due to the spring elongation  $X_2(t) - X_1(t)$  iii) the random forces due to thermal agitation and collisions with the solvent  $R_i(t)$ ,  $i = 1, 2$ . Writing Newton's equations on the beads yields

$$\begin{aligned} m\ddot{X}_1(t) &= \xi(u(X_1(t), t) - \dot{X}_1(t)) + F(X_2(t) - X_1(t)) + R_1(t), \\ m\ddot{X}_2(t) &= \xi(u(X_2(t), t) - \dot{X}_2(t)) - F(X_2(t) - X_1(t)) + R_2(t), \end{aligned}$$

where  $m$  is the mass of each bead,  $\xi$  the drag coefficient,  $F$  the force due to spring elongation. Adding and subtracting the two above equations, neglecting

inertia leads to

$$\begin{aligned}\dot{X}(t) &= \frac{1}{2}(u(X_1(t), t) + u(X_2(t), t)) + \frac{1}{2\xi}(R_1(t) + R_2(t)), \\ \dot{Q}(t) &= u(X_2(t), t) - u(X_1(t), t) - \frac{2}{\xi}F(Q(t)) + \frac{1}{\xi}(R_2(t) - R_1(t)).\end{aligned}$$

The stochastic term  $R_1(t) + R_2(t)$  is then neglected, while  $R_2(t) - R_1(t)$  is assumed to be proportional to white noise (the formal derivative of Brownian motion). An order one Taylor expansion

$$u(X_i(t), t) \simeq u(X(t), t) + \nabla u(X(t), t)(X_i(t) - X(t)) \quad i = 1, 2,$$

yields

$$\begin{aligned}\dot{X}(t) &= u(X(t), t), \\ \dot{Q}(t) &= \nabla u(X(t), t)Q(t) - \frac{2}{\xi}F(Q(t)) + \frac{2k\theta}{\xi}\dot{B}(t),\end{aligned}$$

where  $k$  is Boltzmann's constant,  $\theta$  the absolute temperature and  $B$  a Wiener process (see for instance [126] for a definition). We now specialize the spring force  $F$  into :

$$\begin{aligned}\text{Hookean springs : } F(q) &= Hq \quad \forall q \in \mathbb{R}^d, \\ \text{FENE springs : } F(q) &= H \frac{q}{1 - \frac{|q|^2}{Q_0}} \quad \forall q \in \mathbb{R}^d, |q| < \sqrt{Q_0},\end{aligned}$$

where  $H$  is the spring stiffness. The case of FENE (Finitely Extensible Nonlinear Elastic) dumbbells prevents the springs to have an elongation greater than  $\sqrt{Q_0}$  which corresponds to the length of the fully elongated chain. A scaling of the spring elongation  $Q(t)$  by  $\sqrt{k\theta/H}$  yields the following stochastic differential equations

$$dX(t) = u(X(t), t)dt, \tag{1.11}$$

$$dQ(t) = \left( \nabla u(X(t), t)Q(t) - \frac{1}{2\lambda}F(Q(t)) \right)dt + \frac{1}{\sqrt{\lambda}}dB(t), \tag{1.12}$$

where  $\lambda = \xi/4H$  is the relaxation time and the spring force  $F$  is now defined by

$$\begin{aligned}\text{Hookean springs : } F(q) &= q \quad \forall q \in \mathbb{R}^d, \\ \text{FENE springs : } F(q) &= \frac{q}{1 - \frac{|q|^2}{b}} \quad \forall q \in \mathbb{R}^d, |q| < \sqrt{b}.\end{aligned}$$

According to [113], the parameter  $b$  is linked to the number of monomer units in the polymer chains. Typical values range from  $b = 10$  to  $b = 1000$ . When  $b$  is

large, FENE dumbbells behave as Hookean dumbbells. The Eulerian equation corresponding to (1.11) (1.12) is

$$dq(x, t, \omega) = \left( -u(x, t) \cdot \nabla q(x, t, \omega) + \nabla u(x, t)q(x, t, \omega) - \frac{1}{2\lambda}F(q(x, t, \omega)) \right) dt + \frac{1}{\sqrt{\lambda}}dB(t, \omega), \quad (1.13)$$

for each  $(x, t)$  belonging to the liquid domain  $D_T$  and for each event  $\omega$  in  $\Omega$ , the space of events. It now remains to provide an expression for the extra-stress tensor  $\sigma$ , see [13] sect. 13.3 for details. This expression is

$$\sigma = \frac{\eta_p}{\lambda} \left( \mathbb{E}(F(q)q^T) - I \right), \quad (1.14)$$

where  $\eta_p$  is the polymer viscosity,  $\mathbb{E}(\cdot)$  the mathematical expectation and  $F(q)q^T$  is the symmetric tensor with coefficients  $F_i(q)q_j$ ,  $i, j = 1, d$ , that is :

$$\begin{aligned} \text{Hookean springs : } F_i(q)q_j &= q_i q_j \quad \forall q \in \mathbb{R}^d, \\ \text{FENE springs : } F_i(q)q_j &= \frac{q_i q_j}{1 - \frac{|q|^2}{b}} \quad \forall q \in \mathbb{R}^d, |q| < \sqrt{b}. \end{aligned}$$

The deterministic formulation corresponding to (1.13) (1.14) is obtained by considering the probability density  $f$  for the dumbbells elongations. Here  $f(x, t, q)dxdq$  denotes the probability of finding a dumbbell at time  $t$ , located between  $x$  and  $x + dx$  having elongation between  $q$  and  $x + dq$ . Following [126, 113, 78] for instance, the probability density  $f$  must satisfy the Fokker-Planck equation

$$\frac{\partial f}{\partial t} + \operatorname{div}_x(uf) + \operatorname{div}_q \left( (\nabla_x u)qf - \frac{1}{2\lambda}F(q)f \right) = \frac{1}{2\lambda} \operatorname{div}_q(\nabla_q f). \quad (1.15)$$

The deterministic counterpart of (1.14) is then

$$\begin{aligned} \text{Hookean springs : } \sigma(x, t) &= \frac{\eta_p}{\lambda} \left( \int_{q \in \mathbb{R}^d} qq^T f(x, t, q) dq - I \right), \\ \text{FENE springs : } \sigma(x, t) &= \frac{\eta_p}{\lambda} \left( \int_{q \in \mathbb{R}^d, |q| < \sqrt{b}} \frac{qq^T}{1 - \frac{|q|^2}{b}} f(x, t, q) dq - I \right). \end{aligned}$$

Finally we mention the reflected dumbbells model [18] which, roughly speaking, stands in between the Hookean and FENE models. In this new model, the dumbbells are subject to a linear spring force as long as the spring elongation does not exceed  $\sqrt{b}$ . When this value is reached, the force is modified to prevent further elongation. The resulting nonlinear force is mathematically expressed as the subdifferential of the convex potential

$$\Pi(q) = \begin{cases} \frac{1}{2}|q|^2, & \text{if } |q| < \sqrt{b} \\ +\infty, & \text{otherwise} \end{cases}$$

so that the corresponding stochastic PDE for the elongation dumbbells becomes, in fact, a reflected stochastic PDE. A comparison of different numerical algorithms in this context is proposed in [18].

### 1.2.2 Link Between Hookean Dumbbells and the Oldroyd-B Model

One of the striking properties of the Hookean dumbbells model is that it leads to the Oldroyd-B model. Indeed, let  $q$  be a solution of (1.13) with  $F(q) = q$ . Ito's formula (see for instance [126]) applied to  $V = \mathbb{E}(qq^T)$  yields

$$V + \lambda \left( \frac{\partial V}{\partial t} + u \cdot \nabla V - \nabla u V - V \nabla u^T \right) = I. \quad (1.16)$$

Inserting into (1.14), we obtain that the extra-stress  $\sigma$  satisfies exactly (1.8). The same formal calculation can be performed using the Fokker-Planck equation. Indeed, let  $F(q) = q$ , multiply (1.15) by  $qq^T$  and integrate with respect to the  $q$  variable, then we obtain that

$$V = \int_{q \in \mathbb{R}^d} qq^T f(x, t, q) dq$$

satisfies (1.16). It should be noted that this formal computation can be justified rigorously and can be extended to the Rouse chain. For instance the Rouse chain with nine beads and eight Hookean springs is equivalent to the eight modes Oldroyd-B model with appropriate relaxation times  $\lambda_i$ ,  $i = 1, 8$ , see sect. 15.3 in [13].

The formal equivalence between Hookean dumbbells and the Oldroyd-B model has been historically used in order to derive macroscopic models arising from this kinetic theory. For instance, the FENE-P model is obtained by setting the springs forces  $F$  and the extra-stress  $\sigma$  to

$$F(q) = \frac{q}{1 - \frac{\mathbb{E}(|q|^2)}{b}} \quad \text{and} \quad \sigma = \frac{\eta_p}{\lambda} \left( \frac{\mathbb{E}(qq^T)}{1 - \frac{\mathbb{E}(|q|^2)}{b}} - I \right).$$

Let  $V = \mathbb{E}(qq^T)$ ,  $tr(V) = \mathbb{E}(|q|^2)$ . Using again formal stochastic calculus, we obtain

$$\frac{V}{1 - \frac{tr(V)}{b}} + \lambda \left( \frac{\partial V}{\partial t} + u \cdot \nabla V - \nabla u V - V \nabla u^T \right) = I,$$

the extra-stress being now defined by

$$\sigma = \frac{\eta_p}{\lambda} \left( \frac{V}{1 - \frac{tr(V)}{b}} - I \right).$$

The FENE model has no macroscopic counterpart. However, using expansions of the probability density  $f$  in powers of  $\lambda$  yields the retarded motion model, see for instance sect. 13.5 in [13] or [38]. We also refer to [41] for recent, high order approximations of FENE dumbbells.

Due to the increase of computers power, mesoscopic models have been solved numerically in order to obtain more realistic results, see [76] for a review. Both the deterministic and stochastic formulations of this kinetic theory have been considered. We now discuss which of the two formulations should be used when performing numerical simulations of viscoelastic flows with dumbbells or chains.

For dumbbells, the kinetic variable  $q(.,.,.) \in \mathbb{R}^d$ ,  $d = 2, 3$ , and it is not clear which of the deterministic or stochastic formulations is in principle more efficient from the computational point of view. For chains, that is to say when considering several beads connected by springs, the stochastic formulation should be more efficient than the deterministic one, for the reasons detailed hereafter.

Consider a chain with  $N$  springs and  $N + 1$  beads, then the kinetic variable  $q(.,.,.) \in \mathbb{R}^{d \times N}$ ,  $d = 2, 3$ . The stochastic formulation of a chain leads to a stochastic differential equation similar to (1.13) and to an expression of the extra-stress similar to (1.14). The Monte-Carlo method is used to approach the expectation

$$\mathbb{E}\left(F(q)q^T\right) \simeq \frac{1}{M} \sum_{m=1}^M F(q_m)q_m^T,$$

where the  $q_m$ ,  $m = 1, \dots, M$ , are independent copies of the stochastic process  $q$ . Assuming the velocity  $u(x, t)$  to be a known quantity at a given point  $(x, t)$  in the space-time domain, both the number of degrees of freedom and the computational cost required to solve (1.13) and (1.14) is  $O(dNM)$ , the convergence rate being  $O(M^{-1/2})$  from the central limit theorem. On the other side, the deterministic formulation (1.15) requires a grid of  $\mathbb{R}^{dN}$ . If the grid is uniform with mesh size  $h$ , then the number of degrees of freedom is  $O(h^{-dN})$ , the computational cost is at least the same and the rate of convergence of the error is  $O(h^r)$  depending on the method used (for instance  $r = 2$  when using standard order two centered finite differences). Therefore, the rate of convergence is the same in both methods provided  $h^r = O(M^{-1/2})$  and the number of degrees of freedom of the deterministic method is then  $O(M^{dN/2r})$ . We thus conclude that the Monte-Carlo method is favorable if  $dN \geq 2r$ , that is to say with long chains.

Recently, the sparse tensor product method has been proposed in order to solve parabolic equations in high dimensions [143, 61]. When applied to (1.15), the number of degrees of freedom could be reduced from  $O(h^{-dN})$  to  $O(h^{-1}|\log h|^{dN-1})$  without error increase, so that the method could be competitive with long chains, see for instance [39].

### 1.3 Initial and Boundary Conditions

Let us go back to the free surface problem described at the beginning of this chapter, namely (1.4), (1.5), (1.7), supplemented by the macroscopic model (1.8) or by the mesoscopic model (1.13) (1.14). We now discuss initial and boundary conditions for these two problems.

Inflow conditions :  
 $\varphi, u, \sigma$  (or  $q$ )

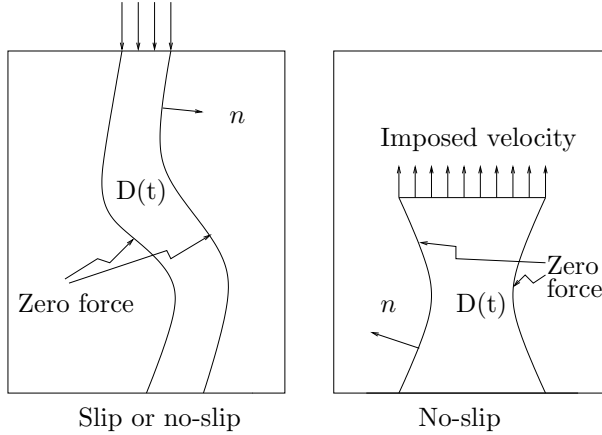


Figure 1.5: Boundary conditions. Left : filling of a cavity with a viscoelastic jet. Right : stretching of a viscoelastic filament. The liquid domain at time  $t$  is  $D(t)$ .

At initial time, the characteristic function of the liquid region  $\varphi(0) : \Lambda \rightarrow \mathbb{R}$  is prescribed, which defines the initial liquid region  $D(0)$ . The velocity field in the liquid region  $u(0) : D(0) \rightarrow \mathbb{R}^d$  is then prescribed. When considering macroscopic models (the Oldroyd-B model (1.8) for instance), the initial extra-stress  $\sigma(0) : D(0) \rightarrow \mathbb{R}^d$  is also prescribed. When dumbbells are considered, eq. (1.13) and (1.14), the initial elongation  $q(0)$  - a stochastic variable - is also prescribed. In general, initial conditions correspond to zero extra-stress that is a  $\mathcal{N}(0, I)$  random variable (a normal distribution with zero mean and unit variance) for  $q(0)$ .

Let us now consider the boundary conditions. For the sake of clarity, two test cases are considered, namely the filling of a cavity with a viscoelastic jet and the stretching of a viscoelastic filament, see Fig. 1.5.

The boundary conditions for the velocity field are the following. It is assumed that no external forces act on the liquid-air free surface, effects of surface tension are neglected, so that

$$-pn + (2\eta_s \epsilon(u) + \sigma)n = 0, \quad (1.17)$$

where  $n$  is the unit outer normal of the liquid-air free surface. On the boundary of the liquid domain being in contact with the walls, either slip, imposed or no-slip (that is  $u = 0$ ) boundary conditions apply. Slip boundary conditions correspond to zero normal velocity  $u \cdot n = 0$  and zero tangent stress

$$\left( -pn + (2\eta_s \epsilon(u) + \sigma)n \right) \cdot t = 0,$$

where  $t$  is the unit outer vector tangent to the boundary of the cavity (two tangent vectors are to be considered in three space dimensions).

Let us now consider a macroscopic model, for instance the Oldroyd-B model (1.8). We define the inflow boundary

$$\{x \in \partial\Lambda \cap \partial D(t); u(x, t) \cdot n(x, t) < 0\}.$$

Since eq. (1.7) and (1.8) are transport equations, both  $\varphi$  and  $\sigma$  are to be imposed at the inflow boundary. Similarly, when considering the mesoscopic dumbbells model (1.13) and (1.14), both  $\varphi$  and  $q$  are to be imposed at the inflow boundary.

## 1.4 Summary

The mathematical models considered in this contribution are the (macroscopic) Oldroyd-B model and the (mesoscopic) FENE dumbbells model.

Given a cavity containing an Oldroyd-B fluid, the free surface model consists in finding the characteristic function of the liquid  $\varphi$ , the velocity  $u$ , pressure  $p$  and extra-stress  $\sigma$  in the liquid satisfying (1.4), (1.5), (1.7) and (1.8), with appropriate initial and boundary conditions.

Alternatively, the free surface FENE dumbbells model consists in finding the characteristic function of the liquid  $\varphi$ , the velocity  $u$ , pressure  $p$ , extra-stress  $\sigma$  and dumbbells elongations  $q$  in the liquid satisfying (1.4) (1.5) (1.7), (1.13) and (1.14), with appropriate initial and boundary conditions.



## Chapter 2

# Numerical Analysis of Simplified Problems

Our goal is now to design a numerical method for solving viscoelastic flows with complex free surfaces. Following [58], an operator splitting method is used for the time discretization. The prediction step consists in solving convection problems only. Then, the new liquid domain is obtained and the correction step consists in solving a viscoelastic flow problem (either macroscopic or mesoscopic) without convection and in a prescribed domain.

In the next section, we propose a review of numerical methods for viscoelastic flows, with emphasis on finite elements. Then, the splitting algorithm is proposed in sect. 2.2, which allows convection to be decoupled from the other physical phenomena. In sect. 2.3 we present some results pertaining to the so-called three fields Stokes problem. Finally, we propose an existence and convergence result for the problem involved in the correction step of the splitting algorithm. The corresponding Oldroyd-B problem is considered in sect. 2.4, the Hookean dumbbells problem in sect. 2.5.

### 2.1 Numerical Models for Viscoelastic Flows : a Chronological Review

#### 2.1.1 Numerical Computations

**Macroscopic Models** Following [37], the first papers reporting numerical computations of viscoelastic flows in two space dimensions were published in the mid seventies. The finite element method became rapidly a method of choice in order to compute flows past submerged obstacles or contractions, and flows with simple free surfaces, die swell for instance. In the early eighties, the increase of computer power allowed mesh refinement but numerical oscillations were soon reported [36, 106, 12]. A typical choice at the time was to use Galerkin finite elements on quadrilaterals (no upwinding), with continuous functions, piecewise

quadratic/linear for the velocity/pressure (the famous  $Q_2 - P_1$  stable element, see [57]) and continuous, piecewise quadratic stresses.

Rapidly, researchers came across the so-called high Deborah/Weissenberg number problem. Here the Deborah/Weissenberg number  $We$  is a dimensionless number measuring the elastic behaviour of the flow  $We = \lambda V/L$ , where  $\lambda$  is the relaxation time present in the Oldroyd-B constitutive equation (1.8),  $V$  a characteristic velocity and  $L$  a characteristic length. Quoting [37] in 1983, “There is no doubt that presently the outstanding problem in the numerical simulation of viscoelastic flows concerns the upper limit on the nondimensional parameter  $W$  (found in all published works) above which the numerical algorithms fail to converge (...) The limit is relatively low, so low in fact that many of the important and dramatic experimental results fall outside the present scope of numerical simulation (...) The limit on  $W$  is common to all published works. It applies to finite-difference or finite-element techniques, to differential and integral constitutive models, and to flows with and without abrupt changes in geometry. Some suggestions for possible causes of the  $W$  barrier are the bifurcation phenomena, the unsuitability of the constitutive models, and the failure of the iterative numerical schemes.”

In [74], the 4:1 axisymmetric contraction flow of upper convected Maxwell and Leonov fluids is computed and the influence of mesh refinement is discussed, five meshes being used. The limit on  $We$  was clearly depending on the mesh size. In [25], on the same test case, the limit on  $We$  was decreasing with mesh size. This phenomena disappeared when smoothing the reentrant corner of the contraction. Still in [25], on the eccentric rotating cylinder test case, a bifurcation point was clearly identified for large  $We$  numbers. The use of upwinding techniques was advocated in order to discretize the transport term  $u \cdot \nabla \sigma$  in the constitutive equation (1.8).

The SUPG method was introduced in [102] in the framework of viscoelastic flows. In the same paper, the  $Q_2 - P_1$  finite element was used for the velocity-pressure approximation, each quadrangle was cut into  $4 \times 4$  smaller quadrangles and the extra-stress was continuous, piecewise linear in each of these small quadrangles. Later, this finite element was proved to be stable and convergent (in the sense of the inf-sup condition) for the three fields Stokes problem [55], see also sect. 2.3 hereafter.

Discontinuous stresses were introduced in [54] for quadrangular elements. The velocity was continuous, piecewise quadratic, the pressure was discontinuous, piecewise linear so that the element satisfies the inf-sup condition for the Stokes problem. The extra-stress was discontinuous, piecewise quadratic and the Lesaint-Raviart upwinding technique was used [88].

The so-called EVSS (Elastic Viscous Split Stress) method enabled the use of low order finite elements for the extra-stress, we refer for instance to [3] for a review paper. The idea of EVSS was to add to the set of equations a new unknown  $d$  such that  $d = \epsilon(u)$ , for stability purposes. The analysis of [53] proved that low order finite elements could be used for the extra-stress, while keeping inf-sup stable elements for the velocity-pressure only. The link with stabilized (Galerkin Least Square) formulations was proposed in [23].

High order elements were also considered to compute viscoelastic flows. For instance, high order methods were considered in [48, 31] for the flow of a falling sphere in a cylindrical tube, the same limit on  $We$  was found in both papers. Spectral elements for time-dependent viscoelastic flows were studied in [51]. Finite volume methods have also been successfully employed for solving viscoelastic flows, with the same limitations of the  $We$  number, see for instance [107, 1].

Nowadays, the high Deborah/Weissenberg number problem is still under debate. For instance, the high resolution parallel computations performed in [77] for the planar 4:1 contraction flow still report decreasing  $We$  with decreasing mesh size. Apparently, this phenomena seems to disappear with the corotational Maxwell model [132]. This numerical observation is consistent with the fact that, from the mathematical viewpoint the corotational Maxwell model is particular, see sect. 2.1.3. Also, when the re-entrant corner is rounded-off with a small radius, accurate spectral computations [52] have shown that instabilities disappear. A numerical scheme satisfying an  $L^1$  estimate and positive-definiteness of the extra-stress was proposed in [99, 86]. However, numerical results [30] confirmed a limiting Deborah/Weissenberg number when using the scheme proposed in [99]. Computations with high Deborah/Weissenberg numbers were recently performed in [66] using a log-based evolution equation, although mesh convergence was not certified. In [144], the flow past a cylinder is considered at high Weissenberg numbers, using a prescribed velocity field. Boundary layers of size  $O(We^{-5})$  are obtained, showing that extremely small mesh size is required in order to compute the stress with sufficient accuracy. Also, a stabilization by jump of the gradients coupled with a nonlinear artificial viscosity shock-capturing type has been introduced in [14] increasing the Weissenberg number limit. Finally, a defect correction method was advocated in [141, 45] in order to reach high Weissenberg numbers for the planar 4:1 contraction flow.

**Mesoscopic Models** Until 1993, the kinetic theory of liquid polymers was evaluated on simple flows (shear, extension), the velocity gradient being a known, prescribed quantity. In 1993, the stochastic formulation of FENE dumbbells model was solved numerically for planar shear flow [83], the velocity field and dumbbells elongations being coupled for the first time. The goal of solving the kinetic theory was to obtain more realistic results with mesoscopic models and, eventually, to circumvent the high Deborah/Weissenberg number problem. In [49, 84], two-dimensional Lagrangian computations were presented, Eulerian computations were proposed in [67, 64] and showed to be more efficient. The use of variance reduction techniques was clearly demonstrated in [114, 20, 73, 21, 22]. The Heterogeneous Multiscale Method was applied in [89] to the framework of FENE dumbbells in one and two space dimensions.

The deterministic formulation of FENE dumbbells was also considered. An efficient spectral element method was used in [98] for coupling the mass and momentum equations to the Fokker-Planck equation (1.15).

Mesoscopic computations have been extended to more complex models such

as chains [80], reptations models, see the review paper [76] and the references therein. These methods are first attempts towards more realistic models. We refer to [81] for a general physical picture of “micro-macro” models for polymers.

### 2.1.2 Mathematical Analysis

**Notations** For simplicity, the notations will be abridged as follow whenever there is no possible confusion. Let  $D$  be a domain of  $\mathbb{R}^d$ ,  $d = 2, 3$ . For a real number  $1 \leq p < +\infty$  (resp.  $p = \infty$ ),  $L^p(D)$  denotes the space of  $p$ -power integrable functions (resp. essentially bounded functions) defined on  $D$  with values in  $\mathbb{R}$ ,  $\mathbb{R}^d$  or  $\mathbb{R}^{d \times d}$ . Also, for a positive integer  $m$ , a real number  $1 \leq p \leq +\infty$ ,  $W^{m,p}(D)$  denotes the usual corresponding Sobolev space, that is the space of functions defined on  $D$  with derivative up to  $m$ -th order in  $L^p(D)$ . When  $p = 2$ , these spaces are the Hilbert spaces denoted as  $H^m(D)$ . As usual, the space  $H_0^1(D)$  denotes the space of  $H^1(D)$  velocities vanishing on the boundary  $\partial\Omega$ , whereas  $L_0^2(D)$  denotes the space of  $L^2(D)$  pressures with zero mean. The dual of  $H_0^1(D)$  is denoted by  $H^{-1}(D)$ . Then, the notation  $(\cdot, \cdot)_D$  stands for the  $L^2(D)$  scalar product for scalar, vectors or tensors, with induced norm  $\|\cdot\|_{L^2(D)}$ .

Given  $T > 0$ , a Banach space  $B$  and a positive integer  $m$ , the space of functions defined on  $[0, T]$  with values in  $B$ , continuous, with (time) derivatives up to  $m$ -th order also continuous is denoted by  $C^m([0, T]; B)$ . Also, for a positive integer  $m$  and a real number  $0 < \mu < 1$ ,  $C^{m+\mu}([0, T]; B)$  stands for the corresponding Hölder space whereas  $h^{m+\mu}([0, T]; B)$  stands for the little Hölder space, see for instance [100] for a definition. For a real number  $1 \leq p \leq +\infty$ ,  $L^p(0, T; B)$  denotes the standard Bochner space. Finally, for a positive integer  $m$ , a real number  $1 \leq p \leq +\infty$ ,  $W^{m,p}(0, T; B)$  is the space of functions defined on  $[0, T]$  with values in  $B$  having (time) derivatives up to  $m$ -th order in  $L^p(0, T; B)$ .

**Macroscopic Models** From the mathematical point of view, the high Deborah/Weissenberg number problem translates into the fact that no a priori estimates are available in adequate norms. Indeed, consider the Oldroyd-B problem (1.4), (1.5) and (1.8), in a prescribed domain  $D$  with  $u = 0$  on the boundary, take the weak formulation and choose  $u$ ,  $p$  and  $\sigma$  as test functions. The following formal estimate is then obtained

$$\begin{aligned} \frac{\rho}{2} \frac{d}{dt} \|u\|_{L^2(D)}^2 + 2\eta_s \|\epsilon(u)\|_{L^2(D)}^2 + \frac{\lambda}{2\eta_p} \frac{d}{dt} \|\sigma\|_{L^2(D)}^2 + \frac{1}{2\eta_p} \|\sigma\|_{L^2(D)}^2 \\ = \frac{\lambda}{2\eta_p} \int_D \text{tr}((\nabla u \sigma + \sigma \nabla u^T) \sigma), \quad (2.1) \end{aligned}$$

which is not sufficient to obtain global existence for any data using energy methods.

The mathematical analysis of macroscopic viscoelastic flows started in 1985 with the study of the change of type (elliptic/hyperbolic) in the upper convected Maxwell model [69]. The existence of a strong solution to the steady flow of an

upper convected Maxwell fluid in differential form was proved in [122]. More precisely, given a smooth bounded domain  $D$  of  $\mathbb{R}^3$ , given an integer  $m \geq 1$ , given  $f \in H^m(D)$  sufficiently small, there exists a stationary solution

$$u \in H^{m+2}(D), \quad p \in H^{m+1}(D), \quad \sigma \in H^{m+1}(D),$$

of (1.4), (1.5) and (1.8) with  $\eta_s = 0$ . Extensions to Oldroyd-B (with several relaxation modes), Giesekus and Phan-Thien Tanner fluids were also proposed. The same technique was used in [123] to prove existence of the K-BKZ integral model.

Existence for the time-dependent flow of an Oldroyd-B fluid has been first addressed in [62]. Local existence of strong solutions was proved, so as global existence for small data. More precisely, given a smooth bounded domain  $D$  of  $\mathbb{R}^3$ , given the final time  $T > 0$ , given initial velocity  $u_0 \in H^2(D) \cap H_0^1(D)$ , initial extra-stress  $\sigma_0 \in H^2(D)$  and source term  $f \in L^\infty(0, T; H_0^1(D))$ ,  $\partial f / \partial t \in L^\infty(0, T; H^{-1}(D))$ , sufficiently small in their respective spaces, there exists a solution

$$u \in L^2(0, T; H^3(D)), \quad \frac{\partial u}{\partial t} \in L^2(0, T; H^1(D)), \quad (2.2)$$

$$p \in L^2(0, T; H^2(D)), \quad \sigma \in C^1(0, T; H^2(D)) \quad (2.3)$$

of (1.4), (1.5) and (1.8) when  $\eta_s > 0$ . Extensions to Jeffreys fluids can be found in [63]. The case of exterior problems is considered in [111]. Generalizations to Banach spaces and a review can be found in [50]. A necessary condition for blow up is provided in [32].

Existence of a weak solution for any data has been proved in [95], but for the corotational Oldroyd-B model only. The case of the corotational Oldroyd-B model is particular since the write hand side in (2.1) must be replaced by

$$\frac{\lambda}{4\eta_p} \int_D \text{tr} \left( (\sigma(\nabla u - \nabla u^T) - (\nabla u - \nabla u^T)\sigma) \sigma \right),$$

which cancels. We also refer to [97, 94] for related work.

In [99, 86], it is noted that, taking the trace of (1.8), yields an  $L^1(D)$  estimate for the extra-stress. However, this estimate does not seem to be sufficient to prove the well-posedness of the Oldroyd-B problem for any data. Estimates involving log-Sobolev inequalities can be found in [65]. An example of non integrable extra-stress for high Deborah/Weissenberg numbers can be found in [131].

**Mesoscopic Models** The mathematical analysis of mesoscopic models started in 1991. Existence of a solution for a deterministic nonlinear dumbbells problem was obtained in [124]. The solvent viscosity was zero and the FENE formulation was not included in the theory. The complete analysis and numerical analysis of a one-dimensional (stochastic) Hookean dumbbells problem was proposed in [71], see also [42] for a similar study.

Existence of a solution for FENE dumbbells (still in one space dimension) was proposed in [72]. Existence of a non-linear (stochastic) dumbbells problem in  $[0, 1]^d$  with periodic boundary conditions was proposed [43], however the analysis does not apply to FENE dumbbells. A similar result was obtained in [90] for the corresponding deterministic formulation. The analysis of the transport term in the dumbbells equations was proposed in [85]. The well posedness of the FENE deterministic equation (without coupling with the mass and momentum equations) was considered in [41]. The well posedness of a modified deterministic dumbbells problem (including the FENE formulation) was considered in [9, 10]. Existence of a weak solution could be proved provided the gradient of the velocity field in the Fokker-Planck equation (1.15) was mollified. See also [147] where same techniques are applied to the Hookean dumbbells model. Local existence of the deterministic FENE dumbbells model was obtained in [146]. In [70], it was proved that convergence to a stationary solution could be obtained for FENE dumbbells whereas Hookean dumbbells are unstable. In [65], new entropy estimates involving log-Sobolev inequalities are proved for FENE dumbbells. Existence of a weak solution of the deterministic corotational FENE dumbbells model has been proved for any data in [96, 93].

### 2.1.3 Numerical Analysis

**Macroscopic Models** To the author's knowledge, the first finite element analysis pertaining to viscoelastic flows in two space dimensions was published in 1989 [55]. The so-called three fields Stokes problem was considered, setting  $\partial\sigma/\partial t = 0$ ,  $\eta_s = 0$  and  $\lambda = 0$  in (1.4), (1.5) and (1.8) to obtain :

$$-\operatorname{div} \sigma + \nabla p = f, \quad \operatorname{div} u = 0, \quad \sigma - 2\eta_p \epsilon(u) = 0.$$

It was proved that the continuous  $Q_2 - P_1 - 16Q_1$  finite element proposed in [102] was stable (in the sense of Brezzi's inf-sup condition) and convergent with optimal order. More precisely, let  $h$  be the typical mesh size and let  $u_h, p_h, \sigma_h$  be the finite element approximations of  $u, p, \sigma$ , respectively. Then, the following a priori error estimate holds :

$$\begin{aligned} \|u - u_h\|_{H^1(D)} + \|p - p_h\|_{L^2(D)} + \|\sigma - \sigma_h\|_{L^2(D)} \\ \leq Ch^2 \left( \|u\|_{H^3(D)} + \|p\|_{H^2(D)} + \|\sigma\|_{H^2(D)} \right), \end{aligned}$$

where  $C$  is independent of the mesh size  $h$  and of the exact solution  $u, p, \sigma$ .

Convergence of a finite element discretization for the Oldroyd-B (nonlinear) stationary problem corresponding to (1.4), (1.5) and (1.8) was first proved in [6], the transport term being disregarded in the momentum equation. Triangular elements were considered, the velocity/pressure being continuous piecewise quadratic/linear, the extra-stress was discontinuous piecewise linear so that the element was stable for the three fields Stokes problem. Moreover, the transport term in the extra-stress constitutive equation was discretized using the method of Lesaint and Raviart [88]. Assuming that  $\eta_s > 0$  and that the solution  $(u, p, \sigma)$

of the continuous problem was small in the  $H^3(D) \times H^2(D) \times H^2(D)$  norm, the authors proved existence and uniqueness of a finite element solution in a  $O(h^{3/2})$  neighbourhood of  $(u, p, \sigma)$ , so as an optimal  $O(h^{3/2})$  convergence rate in the  $H^1(D) \times L^2(D) \times L^2(D)$  norm.

Other finite element spaces were considered in [128, 129] for the three fields Stokes problem and in [130] for the Oldroyd-B stationary problem. A numerical algorithm decoupling velocity/pressure and extra-stress computations was analysed in [108].

Convergence of a space-time discretization for the time-dependent Oldroyd-B model was first considered in [8]. An implicit Euler scheme was considered for the time discretization, together with triangular finite elements (continuous, piecewise quadratic/linear velocity/pressure, discontinuous piecewise linear extra-stress). Assuming that  $\eta_s > 0$  and that the solution  $(u, p, \sigma)$  of the continuous problem was small in the norm

$$\begin{aligned} & \left( \mathcal{C}^1(0, T; H^3(D)) \cap \mathcal{C}^2(0, T; L^2(D)) \right) \\ & \quad \times \mathcal{C}^0(0, T; H^2(D)) \\ & \quad \times \left( \mathcal{C}^1(0, T; H^2(D)) \cap \mathcal{C}^2(0, T; L^2(D)) \right), \end{aligned}$$

assuming the stability condition  $\Delta t \leq C_1 h^{3/2}$  between the time step and the mesh size, the authors proved existence and an optimal convergence rate

$$\begin{aligned} & \left( \Delta t \sum_{n=0}^N \|u(t^n) - u_h^n\|_{H^1(D)}^2 \right)^{1/2} + \left( \Delta t \sum_{n=0}^N \|p(t^n) - p_h^n\|_{L^2(D)}^2 \right)^{1/2} \\ & \quad + \left( \Delta t \sum_{n=0}^N \|\sigma(t^n) - \sigma_h^n\|_{L^2(D)}^2 \right)^{1/2} \leq C(h^{3/2} + \Delta t), \end{aligned}$$

with  $C$  independent of the mesh size  $h$  and time step  $\Delta t$ . Other results pertaining to the numerical analysis of time-dependent problems were obtained in [133, 101, 44, 46, 11].

The convergence of high order methods, more precisely  $hp$  methods, for the three fields Stokes problem was performed in [135].

A posteriori error estimates have been proposed for instance in [68, 115, 116, 109, 47].

**Mesoscopic Models** The numerical analysis of mesoscopic models is recent. Since the Hookean dumbbells model is formally equivalent to the Oldroyd-B problem (see sect. 1.2.2), it is expected that a space discretization which is convergent for macroscopic models should also be convergent for mesoscopic models. This conjecture has been observed in numerical computations but, up to the author's knowledge, there is no convergence proof for FENE dumbbells in two or three space dimensions.

In [71, 87] the complete analysis and numerical analysis of the Hookean dumbbells problem is performed in the framework of a one dimensional shear flow. The error due to time and space discretization is considered, the analysis of the Monte Carlo method is also included. A similar study can be found in [42]. For the sake of clarity, we briefly report hereafter some of the results obtained in [71, 87].

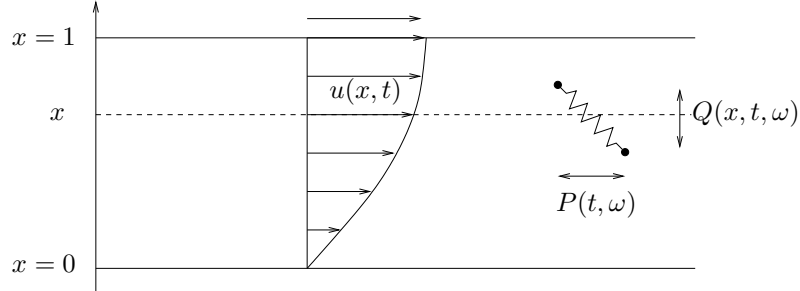


Figure 2.1: Hookean dumbbells in a Couette flow.

Consider the shear flow of an Hookean dumbbells fluid between two parallel infinite planes, the lower plane being at rest, the upper plane moving at imposed velocity, see Fig. 2.1. Let  $u(x, t)$  be the horizontal velocity,  $P(t, \omega)$  and  $Q(x, t, \omega)$  be the horizontal and vertical dumbbell elongation ( $\omega \in \Omega$  the space of events). Then, after a lifting of the boundary conditions, equations (1.4), (1.5), (1.13) and (1.14) with  $F(q) = q$  reduce to

$$\rho \frac{\partial u}{\partial t} - \eta_s \frac{\partial^2 u}{\partial x^2} - \frac{\eta_p}{\lambda} \frac{\partial}{\partial x} \mathbb{E}(PQ) = f, \quad (2.4)$$

$$dP(t, \omega) = -\frac{1}{2\lambda} P(t, \omega) dt + \frac{1}{\sqrt{\lambda}} dV(t, \omega), \quad (2.5)$$

$$dQ(x, t, \omega) = \left( \frac{\partial u}{\partial x}(x, t) P(t, \omega) - \frac{1}{2\lambda} Q(x, t, \omega) \right) dt + \frac{1}{\sqrt{\lambda}} dW(t, \omega), \quad (2.6)$$

where  $V$  and  $W$  are two independent Wiener processes and  $f$  is due to the lifting of the boundary conditions. From the mathematical viewpoint, the shear flow simplifies considerably the model since the quadratic terms analogous to  $\nabla u \sigma + \sigma \nabla u^T$  in (1.8) disappeared. Indeed, since  $P$  is given by

$$P(t, \omega) = e^{-t/2\lambda} P(0, \omega) + \int_0^t e^{-(t-s)/2\lambda} dV(s, \omega),$$

the term  $\partial/\partial x \mathbb{E}(PQ)$  in (2.4) and  $\partial u/\partial x P$  in (2.6) are linear rather than quadratic. Formal a priori estimates can be obtained. Indeed, taking the weak formulation corresponding to (2.4), choosing  $u$  as a test function, we obtain

$$\frac{\rho}{2} \frac{d}{dt} \|u\|_{L^2(0,1)}^2 + \eta_s \|\frac{\partial u}{\partial x}\|_{L^2(0,1)}^2 + \frac{\eta_p}{\lambda} \int_0^1 \mathbb{E}(PQ) \frac{\partial u}{\partial x} dx = \int_0^1 f u dx.$$

Using Ito's formula for  $Q^2$  and take the expectation to obtain

$$\frac{1}{2} \frac{d}{dt} \|\mathbb{E}(Q^2)\|_{L^2(0,1)}^2 + \frac{1}{2\lambda} \|\mathbb{E}(Q^2)\|_{L^2(0,1)}^2 = \int_0^1 \mathbb{E}(PQ) \frac{\partial u}{\partial x} dx + \frac{1}{2\lambda}.$$

Multiplying the above equation by  $\eta_p/\lambda$  and summing with the previous one yields an a priori estimate for

$$\|u\|_{L^\infty(0,T;L^2(0,1))} + \left\| \frac{\partial u}{\partial x} \right\|_{L^2(0,T;L^2(0,1))} + \|Q\|_{L^\infty(0,T;L^2(0,1;L^2(\Omega)))}.$$

Existence of a weak solution can be proved in using the Faedo-Galerkin method. The authors of [71, 87] then consider a space, time and Monte Carlo discretization of (2.4)-(2.6). Assuming sufficient regularity of the data and that the time step  $\Delta t$  is small enough, they prove the following convergence rate :

$$\begin{aligned} & \|u(t^N) - u_h^N 1_{\mathcal{A}_N}\|_{L^2(0,1;L^2(\Omega))} \\ & + \left\| \mathbb{E}(P(t^N)Q(t^N)) - \frac{1}{M} \sum_{j=1}^M P^{N,j} Q_h^{N,j} 1_{\mathcal{A}_N} \right\|_{L^1(0,1;L^1(\Omega))} \\ & = O\left(h + \Delta t + \frac{1}{\sqrt{M}}\right). \end{aligned}$$

Here  $t^N = N\Delta t = T$  and  $\mathcal{A}_N$  is the set defined by

$$\mathcal{A}_N = \left\{ \forall k \leq N, \frac{1}{M} \sum_{j=1}^M (P^{N,j})^2 < \frac{13}{20} \frac{1}{\Delta t} \right\}.$$

Similar results have been obtained in [42].

To the author's knowledge, the numerical analysis of mesoscopic models in more than one space dimensions has been addressed only in [91, 15]. In [91], a priori error estimates are obtained for Hookean dumbbells and a finite difference method in  $[0, 1]^d$  with periodic boundary conditions. The space, time and Monte Carlo discretizations are considered. Assuming  $u \in \mathcal{C}^5([0, T] \times D)$ ,  $\Delta t = h^2$  and the Monte Carlo parameter  $M = h^{-\alpha}$ ,  $\alpha > d$ , it was proved that the velocity error in the  $L^\infty(0, T; L^2([0, 1]^d))$  norm was of order  $O(h^2 + \Delta t + 1/M^{(1-\epsilon)/2})$ , after excluding an event with probability depending on

$$\frac{1}{h^d \Delta t} e^{-M} \quad \text{and} \quad \frac{1}{h^d \Delta t} e^{-M^\epsilon},$$

where  $0 < \epsilon < 1$  is an arbitrary small number.

In [16, 15], Hookean dumbbells are considered in a bounded smooth domain  $D$  and a finite element discretization is considered in space. Pathwise results are obtained. It should be noted that the convective terms in (1.4) (1.13) are removed in order to perform the analysis. The reason for disregarding convective terms is motivated by the use of an operator splitting scheme which will be presented in the next section. This analysis will be detailed in sect. 2.5.

## 2.2 Time Discretization : an Operator Splitting Scheme

Let us consider the free surface Oldroyd-B model (1.4), (1.5), (1.7), (1.8) or alternatively the free surface FENE dumbbells model (1.4), (1.5) (1.7), (1.13), (1.14). Following [103, 104, 28, 26, 27, 19], an order one operator splitting scheme is used for the time discretization, which allows advection and diffusion phenomena to be decoupled. We refer for see for instance [58] chap. II and VI.30 for a general description of operator splitting methods.

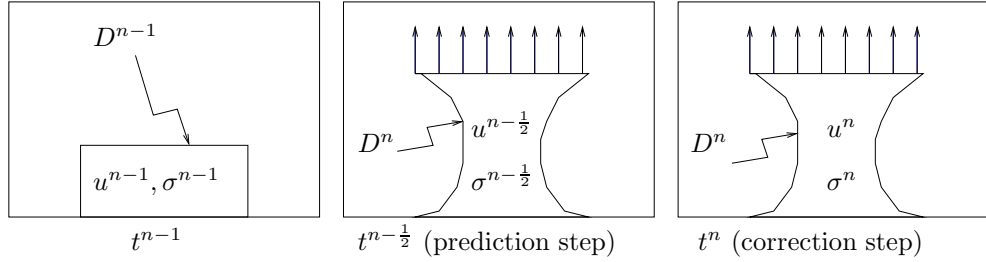


Figure 2.2: The splitting algorithm.

Let  $0 = t^0 < t^1 < t^2 < \dots < t^N = T$  be a subdivision of the time interval  $[0, T]$ , define  $\Delta t^n = t^n - t^{n-1}$  the n-th time step,  $n = 1, 2, \dots, N$ ,  $\Delta t$  the largest time step. At time  $t^{n-1}$ , assume that an approximation  $\varphi^{n-1} : \Lambda \rightarrow \mathbb{R}$  of the volume fraction of liquid is known, which defines the approximation  $D^{n-1}$  of the liquid region at time  $t^{n-1}$  :

$$D^{n-1} = \{x \in \Lambda; \varphi^{n-1}(x) = 1\}.$$

### 2.2.1 The Free Surface Oldroyd-B Model

Consider the free surface Oldroyd-B model (1.4), (1.5), (1.7), (1.8) and assume that approximations of the velocity  $u^{n-1} : D^{n-1} \rightarrow \mathbb{R}^d$  and the extra-stress  $\sigma^{n-1} : D^{n-1} \rightarrow \mathbb{R}^{d \times d}$  are available. Then  $\varphi^n$ ,  $D^n$ ,  $u^n$ ,  $\sigma^n$  are computed by means of a splitting algorithm as illustrated in Fig. 2.2. The prediction step consists in solving three advection problems, which yields the new volume fraction of liquid  $\varphi^n$ , the new liquid region  $D^n$ , the predicted velocity  $u^{n-\frac{1}{2}} : D^n \rightarrow \mathbb{R}^d$  and the predicted extra-stress  $\sigma^{n-\frac{1}{2}} : D^n \rightarrow \mathbb{R}^{d \times d}$ . Then, the correction step is performed, an Oldroyd-B problem without convection is solved in the liquid region  $D^n$ , which yields the new velocity  $u^n : D^n \rightarrow \mathbb{R}^d$ , pressure  $p^n : D^n \rightarrow \mathbb{R}$  and extra-stress  $\sigma^n : D^n \rightarrow \mathbb{R}^{d \times d}$ .

**Prediction Step** The prediction step consists in solving between time  $t^{n-1}$  and  $t^n$  the three advection problems :

$$\frac{\partial \tilde{u}}{\partial t} + (\tilde{u} \cdot \nabla) \tilde{u} = 0, \quad (2.7)$$

$$\frac{\partial \tilde{\sigma}}{\partial t} + (\tilde{u} \cdot \nabla) \tilde{\sigma} = 0, \quad (2.8)$$

$$\frac{\partial \tilde{\varphi}}{\partial t} + \tilde{u} \cdot \nabla \tilde{\varphi} = 0, \quad (2.9)$$

with initial conditions

$$\tilde{u}(t^{n-1}) = u^{n-1},$$

$$\tilde{\sigma}(t^{n-1}) = \sigma^{n-1},$$

$$\tilde{\varphi}(t^{n-1}) = \varphi^{n-1}.$$

These three problems can be solved exactly using the method of characteristics, see for instance [118, 119, 120], the trajectories of the velocity field being straight lines. Indeed, the trajectories are given by  $X'(t) = \tilde{u}(X(t), t)$ , but since  $\tilde{u}$  is constant along the trajectories, we have  $X'(t) = \tilde{u}(X(t^{n-1}), t^{n-1}) = u^{n-1}(X(t^{n-1}))$ . Let  $u^{n-\frac{1}{2}}$ ,  $\sigma^{n-\frac{1}{2}}$ ,  $\varphi^n$  denote the solution at time  $t^n$  of (2.7), (2.8), (2.9), respectively. We thus have

$$u^{n-\frac{1}{2}}(x + \Delta t^n u^{n-1}(x)) = u^{n-1}(x), \quad (2.10)$$

$$\sigma^{n-\frac{1}{2}}(x + \Delta t^n u^{n-1}(x)) = \sigma^{n-1}(x), \quad (2.11)$$

$$\varphi^n(x + \Delta t^n u^{n-1}(x)) = \varphi^{n-1}(x), \quad (2.12)$$

for all  $x$  belonging to  $D^{n-1}$ . Once  $\varphi^n$  is known in the cavity  $\Lambda$ , then the liquid region at time  $t^n$  is defined by :

$$D^n = \{y \in \Lambda; \varphi^n(y) = 1\}. \quad (2.13)$$

**Correction Step** The new liquid region  $D^n$  being known, the predicted velocity  $u^{n-\frac{1}{2}} : D^n \rightarrow \mathbb{R}^d$  and the extra-stress  $\sigma^{n-\frac{1}{2}} : D^n \rightarrow \mathbb{R}^{d \times d}$  being also known, an Oldroyd-B problem without convection is solved :

$$\rho \frac{\partial \hat{u}}{\partial t} - 2\eta_s \operatorname{div} \epsilon(\hat{u}) + \nabla \hat{p} - \operatorname{div} \hat{\sigma} = f, \quad (2.14)$$

$$\operatorname{div} \hat{u} = 0, \quad (2.15)$$

$$\hat{\sigma} + \lambda \left( \frac{\partial \hat{\sigma}}{\partial t} - \nabla \hat{u} \sigma - \sigma \nabla \hat{u}^T \right) = 2\eta_p \epsilon(\hat{u}), \quad (2.16)$$

in the slab  $D^n \times (t^{n-1}, t^n)$ , with initial conditions

$$\hat{u}(t^{n-1}) = u^{n-\frac{1}{2}},$$

$$\hat{\sigma}(t^{n-1}) = \sigma^{n-\frac{1}{2}}.$$

Then the corrected velocity  $u^n : D^n \rightarrow \mathbb{R}^d$  and the extra-stress  $\sigma^n : D^n \rightarrow \mathbb{R}^{d \times d}$  are defined by

$$u^n = \hat{u}(t^n), \quad \sigma^n = \hat{\sigma}(t^n).$$

In sect. 2.4 we discuss the well posedness of the correction step (2.14) (2.15) (2.16). Also, we prove convergence of a finite element discretization in space.

## 2.2.2 The Free Surface FENE Dumbbells Model

In the case of the free surface FENE dumbbells model (1.4), (1.5) (1.7), (1.13), (1.14), given approximations of the velocity  $u^{n-1} : D^{n-1} \rightarrow \mathbb{R}^d$  and the dumbbells elongations  $q^{n-1} : D^{n-1} \times \Omega \rightarrow \mathbb{R}^d$ , the prediction step consists in solving three advection problems, which yields the new volume fraction of liquid  $\varphi^n$ , the new liquid region  $D^n$ , the predicted velocity  $u^{n-\frac{1}{2}} : D^n \rightarrow \mathbb{R}^d$  and the predicted dumbbells elongations  $q^{n-\frac{1}{2}} : D^n \times \Omega \rightarrow \mathbb{R}^d$ . We thus keep (2.10) (2.12) and replace (2.11) by :

$$q^{n-\frac{1}{2}}(x + \Delta t^n u^{n-1}(x), \omega) = q^{n-1}(x, \omega), \quad (2.17)$$

for all  $x$  belonging to  $D^{n-1}$ , for all event  $\omega$  in  $\Omega$ . The new liquid region  $D^n$  is then obtained using (2.13) and the predicted extra-stress  $\sigma^{n-\frac{1}{2}} : D^n \rightarrow \mathbb{R}^{d \times d}$  is defined as :

$$\sigma^{n-\frac{1}{2}} = \frac{\eta_p}{\lambda} \left( \mathbb{E}(F(q^{n-\frac{1}{2}})(q^{n-\frac{1}{2}})^T) - I \right). \quad (2.18)$$

The correction step consists in solving (2.14) (2.15) and replacing (2.16) with

$$d\hat{q} = \left( \nabla u \hat{q} - \frac{1}{2\lambda} F(\hat{q}) \right) dt + \frac{1}{\sqrt{\lambda}} dB, \quad (2.19)$$

$$\hat{\sigma} = \frac{\eta_p}{\lambda} \left( \mathbb{E}(F(\hat{q})\hat{q}^T) - I \right), \quad (2.20)$$

with initial conditions

$$\begin{aligned} \hat{u}(t^{n-1}) &= u^{n-\frac{1}{2}}, \\ \hat{q}(t^{n-1}) &= q^{n-\frac{1}{2}}. \end{aligned}$$

Then the corrected velocity  $u^n : D^n \rightarrow \mathbb{R}^d$ , dumbbells elongations  $q^n : D^n \times \Omega \rightarrow \mathbb{R}^d$  and extra-stress  $\sigma^n : D^n \times \Omega \rightarrow \mathbb{R}^{d \times d}$  are defined by

$$u^n = \hat{u}(t^n), \quad q^n = \hat{q}(t^n), \quad \sigma^n = \frac{\eta_p}{\lambda} \left( \mathbb{E}(F(q^n)(q^n)^T) - I \right).$$

In sect. 2.5 we discuss the well posedness of the correction step (2.14) (2.15) (2.19) (2.20) when  $F(q) = q$  (Hookean dumbbells). Also, we prove convergence of a finite element discretization in space.

## 2.3 The Three Fields Stokes Problem

### 2.3.1 The Continuous Problem

The simplest problem when solving viscoelastic flow problems with finite elements is the three fields Stokes problem obtained by considering the correction step (2.14)-(2.16) setting formally  $\rho = 0$  and  $\lambda = 0$ .

Then, given a domain  $D \subset \mathbb{R}^d$ ,  $d = 2$  or  $3$ , given  $f : D \rightarrow \mathbb{R}^d$  we are looking for  $u : D \rightarrow \mathbb{R}^d$ ,  $p : D \rightarrow \mathbb{R}$  and  $\sigma : D \rightarrow \mathbb{R}^{d \times d}$  such that

$$-2\eta_s \operatorname{div} \epsilon(u) + \nabla p - \operatorname{div} \sigma = f \quad \text{in } D, \quad (2.21)$$

$$\operatorname{div} u = 0 \quad \text{in } D, \quad (2.22)$$

$$\sigma - 2\eta_p \epsilon(u) = 0 \quad \text{in } D, \quad (2.23)$$

$$u = 0 \quad \text{on } \partial D. \quad (2.24)$$

Formally, a smooth solution to this problem satisfies, after elimination of  $\sigma$  :

$$\begin{aligned} -2(\eta_s + \eta_p) \operatorname{div} \epsilon(u) + \nabla p &= f, \\ \operatorname{div} u &= 0. \end{aligned}$$

Therefore, the problem should be well posed even the solvent viscosity  $\eta_s = 0$ , provided  $\eta_p > 0$ . Indeed, existence of a unique weak solution and continuous dependence on the data  $f$  can be proved for  $\eta_s \geq 0$  and  $\eta_p > 0$  using the inf-sup framework [4]. The details can be found in [7, 23] but, for the sake of clarity, we briefly report the arguments hereafter.

As usual, the space  $H_0^1(D)$  denotes the space of  $H^1(D)$  velocities vanishing on the boundary  $\partial\Omega$ , whereas  $L_0^2(D)$  denotes the space of  $L^2(D)$  pressures with zero mean. Recall that  $(\cdot, \cdot)_D$  stands for the  $L^2(D)$  scalar product for scalar, vectors or tensors, with induced norm  $\|\cdot\|_{L^2(D)}$ . The weak formulation corresponding to (2.21)-(2.24) writes : find  $u \in H_0^1(D)$ ,  $p \in L_0^2(D)$ ,  $\sigma \in L^2(D)$  such that

$$2\eta_s(\epsilon(u), \epsilon(v))_D - (p, \operatorname{div} v)_D + (\sigma, \epsilon(v))_D = (f, v)_D \quad \forall v \in H_0^1(D), \quad (2.25)$$

$$(\operatorname{div} u, q)_D = 0 \quad \forall q \in L_0^2(D), \quad (2.26)$$

$$(\sigma - 2\eta_p \epsilon(u), \tau)_D = 0 \quad \forall \tau \in L^2(D). \quad (2.27)$$

Setting  $W = H_0^1(D)^d \times L_0^2(D) \times L^2(D)^{d \times d}$ , we can rewrite this problem as finding  $(u, p, \sigma) \in W$  such that

$$B(u, p, \sigma; v, q, \tau) = F(v, q, \tau) \quad \forall (v, q, \tau) \in W, \quad (2.28)$$

where  $B : W \times W \rightarrow \mathbb{R}$  is the symmetric bilinear form defined by

$$\begin{aligned} B(u, p, \sigma; v, q, \tau) &= 2\eta_s(\epsilon(u), \epsilon(v))_D - (p, \operatorname{div} v)_D + (\sigma, \epsilon(v))_D \\ &\quad - (\operatorname{div} u, q)_D - \frac{1}{2\eta_p}(\sigma, \tau)_D + (\epsilon(u), \tau)_D, \end{aligned}$$

and  $F : W \rightarrow \mathbb{R}$  is the linear form defined by

$$F(v, q, \tau) = (f, v)_D.$$

The space  $W$  is equipped with the norm  $\|\cdot\|_W$  defined for all  $(v, q, \tau) \in W$  by :

$$\|v, q, \tau\|_W^2 = 2(\eta_s + \eta_p)\|\epsilon(v)\|_{L^2(D)}^2 + \frac{1}{2(\eta_s + \eta_p)}\|q\|_{L^2(D)}^2 + \frac{1}{2\eta_p}\|\tau\|_{L^2(D)}^2.$$

Then, the well posedness of (2.28) is a consequence of the following Lemma.

**Lemma 2.1** *The symmetric bilinear form  $B$  satisfies the inf-sup condition, uniformly with respect to  $\eta_s \geq 0$  and  $\eta_p > 0$  :  $\exists C > 0$ ,  $\forall \eta_s \geq 0$ ,  $\forall \eta_p > 0$ ,  $\forall (u, p, \sigma) \in W$*

$$\sup_{(v, q, \tau) \in W \setminus \{0\}} \frac{B(u, p, \sigma; v, q, \tau)}{\|v, q, \tau\|_W} \geq C\|u, p, \sigma\|_W.$$

**Proof** In order to prove that  $B$  satisfies the Babuška inf-sup conditions [4], it suffices to prove that  $\exists C_1, C_2 > 0$ ,  $\forall \eta_s \geq 0$ ,  $\forall \eta_p > 0$ ,  $\forall (u, p, \sigma) \in W$ ,  $\exists (v, q, \tau) \in W$  such that

$$B(u, p, \sigma; v, q, \tau) \geq C_1\|u, p, \sigma\|_W^2 \quad \text{and} \quad \|v, q, \tau\|_W \leq C_2\|u, p, \sigma\|_W. \quad (2.29)$$

Let  $(u, p, \sigma) \in W$ . Clearly, we have

$$\begin{aligned} B(u, p, \sigma; u, -p, -\sigma) &= 2\eta_s\|\epsilon(u)\|_{L^2(D)}^2 + \frac{1}{2\eta_p}\|\sigma\|_{L^2(D)}^2, \\ B(u, p, \sigma; 0, 0, 2\eta_p\epsilon(u)) &= 2\eta_p\|\epsilon(u)\|_{L^2(D)}^2 - (\sigma, \epsilon(u))_D. \end{aligned}$$

On the other side, the classical inf-sup condition between pressure and velocity implies :  $\exists C_3 > 0$ ,  $\forall p \in L_0^2(D)$ ,  $\exists \tilde{v} \in H_0^1(D)$ , such that

$$\|p\|_{L^2(D)}^2 = (p, \operatorname{div} \tilde{v})_D \quad \text{and} \quad \|\epsilon(\tilde{v})\|_{L^2(D)} \leq C_3\|p\|_{L^2(D)},$$

thus we have

$$B(u, p, \sigma; -\tilde{v}, 0, 0) = -2\eta_s(\epsilon(u), \epsilon(\tilde{v}))_D + \|p\|_{L^2(D)}^2 + (\sigma, \epsilon(\tilde{v}))_D.$$

Therefore, for  $\delta > 0$ , we have :

$$\begin{aligned} B(u, p, \sigma; u - \delta\tilde{v}, -p, -\sigma + 2\delta\eta_p\epsilon(u)) \\ &= 2(\eta_s + \delta\eta_p)\|\epsilon(u)\|_{L^2(D)}^2 + \frac{1}{2\eta_p}\|\sigma\|_{L^2(D)}^2 + \delta\|p\|_{L^2(D)}^2 \\ &\quad - (\sigma, \epsilon(u))_D - 2\delta\eta_s(\epsilon(u), \epsilon(\tilde{v}))_D + \delta(\sigma, \epsilon(\tilde{v}))_D, \end{aligned}$$

and we can prove that (2.29) holds with

$$(v, q, \tau) = (u - \delta\tilde{v}, -p, -\sigma + 2\delta\eta_p)$$

provided  $\delta > 0$  is chosen sufficiently small. Please note that  $\delta$  does not depend on  $\eta_s$  or  $\eta_p$ , we refer to [7, 23] for details.

From the above lemma, we deduce that, if  $f \in H^{-1}(D)$ , then the problem is well posed : there exists a unique solution to (2.28) and  $C > 0$  independent of  $f$  such that

$$\|u, p, \sigma\|_W \leq C\|f\|_{H^{-1}(D)}.$$

**Remark 2.1** *The interested reader should note that a different weak formulation was used in [55, 129]. Indeed, (2.25)-(2.27) was considered with  $\eta_s = 0$  and rewritten in the framework of Brezzi inf-sup theorem [24] as finding  $(u, p, \sigma) \in W$  such that*

$$\begin{aligned} a(\sigma, p; \tau, q) + b(\tau, q; u) &= 0 & \forall (\tau, q) \in L^2(D) \times L_0^2(D), \\ b(\sigma, p; v) &= -(f, v)_D & \forall v \in H_0^1(D), \end{aligned}$$

where the bilinear forms  $a$  and  $b$  are defined by

$$a(\sigma, p; \tau, q) = \frac{1}{2\eta_p}(\sigma, \tau)_D \quad \text{and} \quad b(\tau, q; u) = -(\epsilon(u), \tau)_D + (\operatorname{div} u, q)_D.$$

Then,  $a$  and  $b$  satisfy Brezzi's inf-sup conditions, i.e.  $a$  is coercive onto

$$K = \{(\sigma, p) \in L^2(D) \times L_0^2(D) \text{ such that } b(\sigma, p; v) = 0, \forall v \in H_0^1(D)\},$$

and  $b$  satisfies the inf-sup condition

$$\exists C_2 > 0, \forall v \in H_0^1(D) \quad \sup_{(\sigma, p) \in L^2(D) \times L^2(D) \setminus \{0\}} \frac{b(\sigma, p; v)}{\|\sigma, p\|_{L^2(D) \times L^2(D)}} \geq C_2 \|v\|_{H^1(D)},$$

thus the problem is well posed.

### 2.3.2 Finite Element Discretizations

We are now interested in computing finite elements approximations of (2.25)-(2.27) or equivalently (2.28). For any  $h > 0$ , let  $\mathcal{T}_h$  be a finite element mesh of  $D$  into triangles ( $d = 2$ ) or tetrahedrons ( $d = 3$ ), regular in the sense of [34].

**Galerkin Methods** Let  $V_h \subset H_0^1(D)^d$ ,  $Q_h \subset L_0^2(D)$  and  $M_h \subset L^2(D)^{d \times d}$  be finite element subspaces for the velocity, pressure and extra-stress, respectively, let  $W_h = V_h \times Q_h \times M_h$ . A Galerkin method corresponding to (2.28) writes : find  $(u_h, p_h, \sigma_h) \in W_h$  such that

$$B(u_h, p_h, \sigma_h; v_h, q_h, \tau_h) = F(v_h, q_h, \tau_h) \quad \forall (v_h, q_h, \tau_h) \in W_h. \quad (2.30)$$

Clearly, if the finite element spaces satisfy the conditions  $\operatorname{div} V_h \subset M_h$  and

$$\exists C > 0, \forall h > 0, \forall q_h \in Q_h \quad \sup_{v_h \in V_h \setminus \{0\}} \frac{(q_h, \operatorname{div} v_h)}{\|\nabla v_h\|_{L^2(D)}} \geq C \|q_h\|_{L^2(D)}, \quad (2.31)$$

then the discrete analogue of Lemma 2.1 holds since the proof can be reproduced in the discrete space  $W_h$  instead of  $W$ . Thus the problem is well posed and optimal a priori error estimates hold.

An example of spaces  $V_h$ ,  $Q_h$  and  $M_h$  satisfying the two above conditions when  $d = 2$  is the following. The velocity is continuous, piecewise quadratic, thus the velocity divergence is discontinuous piecewise linear, so as the extra-stress. Moreover, the pressure is continuous, piecewise linear, so that (2.31) is satisfied. This finite element discretizations has been used in [6].

**Remark 2.2** Let us consider the framework introduced in Remark 2.1. Following [55, 129], optimal a priori error estimates can be recovered provided the finite element spaces  $V_h$ ,  $Q_h$  and  $M_h$  are such that the bilinear forms  $a$  and  $b$  satisfy Brezzi's discrete inf-sup conditions, uniformly with respect to  $h$ .

An example of spaces  $V_h$ ,  $Q_h$  and  $M_h$  satisfying these two conditions when  $d = 2$  is the following [55]. The velocity, pressure and extra-stress are continuous on quadrangles. The velocity is piecewise quadratic, the pressure piecewise linear. Each quadrangle is cut into  $4 \times 4$  quadrangles and the extra-stress is piecewise linear on these smaller quadrangles. We refer to [129] for a similar example on triangles.

**Stabilized Galerkin Least Square Formulations** Stabilized Galerkin Least Square formulations can be considered in order to avoid compatibility conditions between the finite element spaces  $V_h$ ,  $Q_h$  and  $M_h$ . The simplest stabilized scheme consists in considering continuous, piecewise linear spaces for the velocity, pressure and extra-stress together with the following Galerkin Least Square formulation : find  $(u_h, p_h, \sigma_h) \in W_h = V_h \times Q_h \times M_h$  such that

$$B_h(u_h, p_h, \sigma_h; v_h, q_h, \tau_h) = F_h(v_h, q_h, \tau_h) \quad \forall (v_h, q_h, \tau_h) \in W_h. \quad (2.32)$$

Here  $B_h$  is the bilinear form defined by

$$\begin{aligned} B_h(u_h, p_h, \sigma_h; v_h, q_h, \tau_h) &= B(u_h, p_h, \sigma_h; v_h, q_h, \tau_h) \\ &\quad - \sum_{K \in \mathcal{T}_h} \frac{\alpha h_K^2}{2\eta_p} \left( -2\eta_s \operatorname{div} \epsilon(u_h) + \nabla p_h - \operatorname{div} \sigma_h, \nabla q_h \right)_K \\ &\quad + 2\eta_p \left( \frac{1}{2\eta_p} \sigma_h - \epsilon(u_h), -\epsilon(v_h) \right)_D, \end{aligned} \quad (2.33)$$

and  $F_h$  the linear form defined by

$$F_h(v_h, q_h, \tau_h) = F(v_h, q_h, \tau_h) - \sum_{K \in \mathcal{T}_h} \frac{\alpha h_K^2}{2\eta_p} (f, \nabla q)_K,$$

where  $\alpha > 0$  is a dimensionless parameter and  $(\cdot, \cdot)_K$  denotes the  $L^2(K)$  scalar product. The stabilized scheme (2.32) is designed so that it is stable and consistent. Consistency means that, if the solution  $(u, p, \sigma)$  of (2.28) is smooth

enough, then

$$B_h(u, p, \sigma; v_h, q_h, \tau_h) = F_h(v_h, q_h, \tau_h) \quad \forall (v_h, q_h, \tau_h) \in W_h.$$

The key point for proving stability is stated in the following Lemma.

**Lemma 2.2** *Let  $C_I$  be the largest constant involved in the following inverse inequality*

$$C_I \sum_{K \in \mathcal{T}_h} h_K^2 \| \operatorname{div} \sigma_h \|_{L^2(K)}^2 \leq \| \sigma_h \|_{L^2(D)}^2 \quad \forall \sigma_h \in M_h, \quad (2.34)$$

and let  $0 < \alpha < C_I$ . Then,  $\exists C > 0$ ,  $\forall \eta_s \geq 0$ ,  $\forall \eta_p > 0$ ,  $\forall h > 0$ ,  $\forall (u_h, p_h, \sigma_h) \in W_h$

$$B_h(u_h, p_h, \sigma_h; u_h, -p_h, -\sigma_h) \geq C \|u_h, p_h, \sigma_h\|_h^2,$$

where  $\|\cdot\|_h$  is the discrete norm defined by

$$\begin{aligned} \|u_h, p_h, \sigma_h\|_h^2 &= 2(\eta_s + \eta_p) \|\epsilon(u_h)\|_{L^2(D)}^2 + \frac{1}{2(\eta_s + \eta_p)} \sum_{K \in \mathcal{T}_h} h_K^2 \|\nabla p_h\|_{L^2(K)}^2 \\ &\quad + \frac{1}{2\eta_p} \|\sigma_h\|_{L^2(D)}^2. \end{aligned}$$

**Proof** Let  $(u_h, p_h, \sigma_h) \in W_h$ , we have

$$\begin{aligned} B_h(u_h, p_h, \sigma_h; u_h, -p_h, -\sigma_h) &= 2(\eta_s + \eta_p) \|\epsilon(u_h)\|_{L^2(D)}^2 + \frac{1}{2\eta_p} \|\sigma_h\|_{L^2(D)}^2 \\ &\quad + \sum_{K \in \mathcal{T}_h} \frac{\alpha h_K^2}{2\eta_p} \left( \|\nabla p_h\|_{L^2(D)}^2 - (\operatorname{div} \sigma_h, \nabla p_h)_D \right) - (\sigma_h, \epsilon(u_h))_D. \end{aligned}$$

It then suffices to use (2.34) and Young's inequality to obtain the result. We again refer to [23] for details.

From this Lemma, the discrete analogue of Lemma 2.1 can be proved for the bilinear form  $B_h : \exists C > 0$ ,  $\forall \eta_s \geq 0$ ,  $\forall \eta_p > 0$ ,  $\forall h > 0$ ,  $\forall (u_h, p_h, \sigma_h) \in W_h$

$$\sup_{(v_h, q_h, \tau_h) \in W_h \setminus \{0\}} \frac{B_h(u_h, p_h, \sigma_h; v_h, q_h, \tau_h)}{\|v_h, q_h, \tau_h\|_W} \geq C \|u_h, p_h, \sigma_h\|_W,$$

so that optimal a priori error estimates hold.

**EVSS Stabilization** In [53], an EVSS (Elastic Viscous Split Stress) scheme was analysed. The EVSS scheme consists in adding to the three fields Stokes problem (2.21)-(2.23) a new field  $d$ , for stability purposes, as following :

$$-2(\eta_s + \eta_p) \operatorname{div} \epsilon(u) + \nabla p - \operatorname{div} (\sigma - 2\eta_p d) = f \quad \text{in } D, \quad (2.35)$$

$$\operatorname{div} u = 0 \quad \text{in } D, \quad (2.36)$$

$$\sigma - 2\eta_p \epsilon(u) = 0 \quad \text{in } D, \quad (2.37)$$

$$d - \epsilon(u) = 0 \quad \text{in } D. \quad (2.38)$$

Equal order finite elements were used to approach  $d$  and  $\sigma$  thus, the Galerkin finite element formulation corresponding to (2.35)-(2.38) consists in finding  $(u_h, p_h, \sigma_h, d_h) \in W_h = V_h \times Q_h \times M_h \times M_h$  such that

$$B(u_h, p_h, \sigma_h, d_h; v_h, q_h, \tau_h, e_h) = F(v_h, q_h, \tau_h, e_h) \quad \forall (v_h, q_h, \tau_h, e_h) \in W_h. \quad (2.39)$$

Here  $B$  is the bilinear form defined by

$$\begin{aligned} B(u_h, p_h, \sigma_h, d_h; v_h, q_h, \tau_h, e_h) &= 2(\eta_s + \eta_p)(\epsilon(u_h), \epsilon(v_h))_D - (p_h, \operatorname{div} v_h)_D \\ &\quad + (\sigma_h - 2\eta_p d_h, \epsilon(v_h))_D - (\operatorname{div} u_h, q_h)_D - \frac{1}{2\eta_p}(\sigma_h, \tau_h)_D + (\epsilon(u_h), \tau_h)_D \\ &\quad + 2\eta_p(d_h - \epsilon(u_h), e_h)_D. \end{aligned}$$

Since  $\sigma_h$  and  $d_h$  belong to same finite element space  $M_h$ , it is clear that  $\sigma_h = 2\eta_p d_h$  so that solving (2.39) is equivalent to finding  $(u_h, p_h) \in V_h \times Q_h$  such that

$$\begin{aligned} 2(\eta_s + \eta_p)(\epsilon(u_h), \epsilon(v_h))_D - (p_h, \operatorname{div} v_h)_D \\ - (\operatorname{div} u_h, q_h)_D = (f, v_h)_D \quad \forall (v_h, q_h) \in V_h \times Q_h, \quad (2.40) \end{aligned}$$

and then finding  $\sigma_h \in M_h$  such that

$$(\sigma_h, \tau_h)_D = 2\eta_p(\epsilon(u_h), \tau_h)_D \quad \forall \tau_h \in M_h.$$

Therefore, (2.39) is well posed whenever the finite element spaces  $V_h$  and  $Q_h$  satisfy the classical discrete inf-sup condition (2.31).

The connection between stabilized Galerkin Least Square formulations and EVSS stabilization has been studied for the three fields Stokes problem in [23]. An extension to a simplified stationary Oldroyd-B problem has been considered in [116]. It should be noted that, when considering the Oldroyd-B model or FENE dumbbells, both stabilized Galerkin Least Square and EVSS schemes differ. However, the EVSS formulation is much simpler to implement, therefore it is usually preferred. Numerical simulations of FENE dumbbells using the EVSS scheme have been proposed in [21, 22].

## 2.4 A Simplified Oldroyd-B Problem

This section is devoted to the study of the correction step of the free surface algorithm for the Oldroyd-B problem presented in sect. 2.2. This is (2.14)-(2.16) that are recalled hereafter for the convenience of the reader. Two different considerations are discussed here. First, existence and uniqueness results with small data are presented. Second, the well posedness of a stabilized finite element discretization in space is obtained, so as optimal convergence results. The results presented here can be found in more details in [17].

Let  $D$  be a bounded, connected open set of  $\mathbb{R}^d$ ,  $d \geq 2$  with boundary  $\partial D$  of class  $C^2$ , and let  $T > 0$  be the final time. We consider the following problem.

Given initial conditions  $u_0 : D \rightarrow \mathbb{R}^d$ ,  $\sigma_0 : D \rightarrow \mathbb{R}^{d \times d}$ , a force term  $f$ , a constant density  $\rho > 0$ , constant solvent and polymer viscosities  $\eta_s > 0$ ,  $\eta_p > 0$ , a constant relaxation time  $\lambda > 0$ , find the velocity  $u : D \times (0, T) \rightarrow \mathbb{R}^d$ , pressure  $p : D \times (0, T) \rightarrow \mathbb{R}$  and extra-stress  $\sigma : D \times (0, T) \rightarrow \mathbb{R}^{d \times d}$  such that

$$\rho \frac{\partial u}{\partial t} - 2\eta_s \operatorname{div} \epsilon(u) + \nabla p - \operatorname{div} \sigma = f \quad \text{in } D \times (0, T), \quad (2.41)$$

$$\operatorname{div} u = 0 \quad \text{in } D \times (0, T), \quad (2.42)$$

$$\frac{1}{2\eta_p} \sigma + \frac{\lambda}{2\eta_p} \left( \frac{\partial \sigma}{\partial t} - (\nabla u)\sigma - \sigma(\nabla u)^T \right) - \epsilon(u) = 0 \quad \text{in } D \times (0, T), \quad (2.43)$$

$$u = 0 \quad \text{on } \partial D \times (0, T), \quad (2.44)$$

$$u(\cdot, 0) = u_0, \quad \sigma(\cdot, 0) = \sigma_0 \quad \text{in } D. \quad (2.45)$$

Note that, when comparing to (2.14)-(2.16), the hat symbols have been omitted for clarity purpose.

When  $D$  is of class  $C^2$ , the implicit function theorem has been used in [17] to prove that the above problem admits a unique solution

$$\begin{aligned} u &\in W^{1,q}(0, T; L^r(D)) \cap L^q(0, T; W^{2,r}(D)), \\ p &\in L^q(0, T; W^{1,r}(D)), \\ \sigma &\in W^{1,q}(0, T; W^{1,r}(D)), \end{aligned} \quad (2.46)$$

with  $1 < q < \infty$ ,  $d < r < \infty$ , for any data  $f$ ,  $u_0$ ,  $\sigma_0$  small enough in appropriate spaces. We assume that such a results also holds when  $D$  is a convex polygon, see [116] for a proof in the framework of the corresponding stationary problem. Then, the above regularity is sufficient to ensure the existence and convergence of a stabilized, continuous, piecewise linear finite element discretization in space.

The finite element approximation in space is now introduced. For any  $h > 0$ , let  $\mathcal{T}_h$  be a decomposition of the computational domain  $D$  into triangles  $K$  with diameter  $h_K$  less than  $h$ , regular in the sense of [34]. We consider as in subsection 2.3.2 the finite element spaces  $V_h$ ,  $Q_h$  and  $M_h$  corresponding to continuous, piecewise linear velocity, pressure and extra-stress. We denote  $i_h$  the  $L^2(D)$  projection onto  $V_h$ ,  $Q_h$  or  $M_h$  and introduce the following stabilized finite element discretization in space of (2.41)-(2.45). Given  $f$ ,  $u_0$ ,  $\sigma_0$  find

$$(u_h, p_h, \sigma_h) : t \rightarrow (u_h(t), p_h(t), \sigma_h(t)) \in V_h \times Q_h \times M_h$$

such that  $u_h(0) = i_h u_0$ ,  $\sigma_h(0) = i_h \sigma_0$  and such that the following weak formu-

lation holds in  $]0, T[$  :

$$\begin{aligned} & \rho \left( \frac{\partial u_h}{\partial t}, v_h \right)_D + 2\eta_s \left( \epsilon(u_h), \epsilon(v_h) \right)_D - \left( p_h, \operatorname{div} v_h \right)_D + \left( \sigma_h, \epsilon(v_h) \right)_D \\ & \quad - \left( f, v_h \right)_D + \left( \operatorname{div} u_h, q_h \right)_D + \sum_{K \in \mathcal{T}_h} \frac{\alpha h_K^2}{2\eta_p} \left( \nabla p_h, \nabla q_h \right)_K \\ & \quad + \frac{1}{2\eta_p} \left( \sigma_h, \tau_h \right)_D + \frac{\lambda}{2\eta_p} \left( \frac{\partial \sigma_h}{\partial t} - (\nabla u_h) \sigma_h - \sigma_h (\nabla u_h)^T, \tau_h \right)_D \\ & \quad - \left( \epsilon(u_h), \tau_h \right)_D = 0, \end{aligned} \quad (2.47)$$

for all  $(v_h, q_h, \tau_h) \in V_h \times Q_h \times M_h$ . Here  $\alpha > 0$  is a dimensionless stabilization parameter.

In order to prove that the solution of the nonlinear finite element discretization (2.47) exists and converges to that of (2.41)-(2.45), we shall use the abstract Theorem 2.1 of [29]. For this purpose, we introduce  $X_h$  defined by

$$X_h = L^2(0, T; V_h) \times L^\infty(0, T; M_h)$$

equipped with the norm  $\|\cdot\|_{X_h}$  defined for all  $x_h = (u_h, \sigma_h) \in X_h$  by

$$\|x_h\|_{X_h}^2 = 2\eta_s \int_0^T \|\epsilon(u_h(t))\|_{L^2(\Omega)}^2 dt + \frac{\lambda}{4\eta_p} \sup_{t \in [0, T]} \|\sigma_h(t)\|_{L^2(\Omega)}^2.$$

Then, we rewrite the solution of (2.47) as the following fixed point problem. Given  $y = (f, u_0, \sigma_0) \in Y$ , find  $x_h = (u_h, \sigma_h) \in X_h$  such that

$$x_h = \mathsf{T}_h(y, S(x_h)). \quad (2.48)$$

Here  $Y$  is the functional space corresponding to the data  $(f, u_0, \sigma_0)$  (see [17] for details) and  $S$  is defined by

$$S(x_h) = \frac{\lambda}{2\eta_p} \left( (\nabla u_h) \sigma_h + \sigma_h (\nabla u_h)^T \right)_D.$$

Given  $y = (f, u_0, \sigma_0) \in Y$  and  $g \in L^2(0, T; L^2(D))$ , computing  $\mathsf{T}_h(y, g)$  consists in solving a time dependent three fields Stokes problem discretized in space, namely :

$$\begin{aligned} \mathsf{T}_h : Y \times L^2(0, T; L^2(D)) & \rightarrow X_h \\ (f, u_0, \sigma_0, g) & \rightarrow \mathsf{T}_h(f, u_0, \sigma_0, g) := (\tilde{u}_h, \tilde{\sigma}_h) \end{aligned}$$

where for  $t \in (0, T)$

$$(\tilde{u}_h, \tilde{p}_h, \tilde{\sigma}_h) : t \rightarrow (\tilde{u}_h(t), \tilde{p}_h(t), \tilde{\sigma}_h(t)) \in V_h \times Q_h \times M_h$$

satisfies  $\tilde{u}_h(0) = i_h u_0$ ,  $\tilde{\sigma}_h(0) = i_h \sigma_0$  and

$$\begin{aligned} & \rho \left( \frac{\partial \tilde{u}_h}{\partial t}, v_h \right)_D + 2\eta_s \left( \epsilon(\tilde{u}_h), \epsilon(v_h) \right)_D - \left( \tilde{p}_h, \operatorname{div} v_h \right)_D + \left( \tilde{\sigma}_h, \epsilon(v_h) \right)_D - \left( f, v_h \right)_D \\ & \quad + \left( \operatorname{div} \tilde{u}_h, q_h \right)_D + \sum_{K \in \mathcal{T}_h} \frac{\alpha h_K^2}{2\eta_p} \left( \nabla \tilde{p}_h, \nabla q_h \right)_K \\ & \quad + \frac{1}{2\eta_p} \left( \tilde{\sigma}_h, \tau_h \right)_D + \frac{\lambda}{2\eta_p} \left( \frac{\partial \tilde{\sigma}_h}{\partial t}, \tau_h \right)_D - \left( \epsilon(\tilde{u}_h), \tau_h \right)_D - \frac{\lambda}{2\eta_p} \left( g, \tau_h \right)_D = 0 \end{aligned} \quad (2.49)$$

for all  $(v_h, q_h, \tau_h) \in V_h \times Q_h \times M_h$ , a.e in  $(0, T)$ .

In [17], it is proved that (2.48) has a unique solution converging to that of (2.41)-(2.45). Indeed, following [116], (2.48) is written as the following nonlinear problem : given  $y = (f, u_0, \sigma_0) \in Y$ , find  $x_h = (u_h, \sigma_h) \in X_h$  such that

$$F_h(y, x_h) = 0, \quad (2.50)$$

where  $F_h : Y \times X_h \rightarrow X_h$  is defined by

$$F_h(y, x_h) = x_h - \mathsf{T}_h(y, S(x_h)). \quad (2.51)$$

The abstract Theorem 2.1 of [29] can be then used in order to prove existence and convergence of a solution to (2.50). The mapping  $F_h : Y \times X_h \rightarrow X_h$  is  $\mathcal{C}^1$ . Moreover, the scheme is consistent,  $D_x F_h$  has bounded inverse at  $i_h x$  and  $D_x F_h$  is locally Lipschitz at  $i_h x$ . Here  $i_h$  is the  $L^2(D)$  projection onto the finite element space  $X_h$  and  $x = (u, \sigma)$  is the solution of the continuous problem (2.41)-(2.45), with regularity (2.46). Therefore, applying Theorem 2.1 of [29], existence of a semi-discrete solution  $x_h$  can be proved in the neighbourhood of  $i_h x$  provided the data  $y$  is small enough in  $Y$ , the space of data. Note that this regularity implies that the trajectories  $(x, t) \mapsto q_h(x, t, \omega)$  are continuous, for almost each event  $\omega \in \Omega$ . Moreover, optimal error estimates hold for  $\|x - x_h\|_{X_h}$  that is :

$$\|u - u_h\|_{L^2(0, T; H^1(D))} + \|\sigma - \sigma_h\|_{L^\infty(0, T; L^2(D))} = O(h).$$

We refer to [17] for details.

## 2.5 A Simplified Hookean Dumbbells Problem

As a first step towards the analysis of stochastic models for viscoelastic fluids, this section is devoted to the study of the correction step of the free surface algorithm for Hookean dumbbells model, see sect. 2.2. This is (2.14), (2.15) supplemented by (2.19) and (2.20) with  $F(q) = q$ , that are recalled hereafter for the convenience of the reader. A pathwise existence will be provided with enough regularity to ensure the convergence of the finite element scheme proposed. The results presented here can be found in more details in [16, 15].

We refer to [20, 73] for presentations related to the Monte-Carlo discretization and the use of variance reduction techniques.

Let  $D \subset \mathbb{R}^d$  be the “physical” space,  $T > 0$  be the final time and  $(\Omega, \mathcal{F}, \mathcal{P})$  be a complete filtered probability space. Given  $f : D \times [0, T] \rightarrow \mathbb{R}^d$ ,  $u_0 : D \rightarrow \mathbb{R}^d$  and  $q_0 : \Omega \rightarrow \mathbb{R}^d$ , we are seeking for the velocity  $u : D \times [0, T] \rightarrow \mathbb{R}^d$ , the pressure  $p : D \times [0, T] \rightarrow \mathbb{R}$  and the dumbbells elongation  $q : D \times [0, T] \times \Omega \rightarrow \mathbb{R}^d$  such that

$$\begin{aligned} \rho \frac{\partial u}{\partial t} - 2\eta_s \operatorname{div} \epsilon(u) + \nabla p \\ - \frac{\eta_p}{\lambda} \operatorname{div} (\mathbb{E}(qq^T) - I) = f & \quad \text{in } D \times (0, T), \end{aligned} \quad (2.52)$$

$$\operatorname{div} u = 0 \quad \text{in } D \times (0, T), \quad (2.53)$$

$$dq = \left( \nabla u q - \frac{1}{2\lambda} q \right) dt + \frac{1}{\sqrt{\lambda}} dB \quad \text{in } D \times (0, T) \times \Omega, \quad (2.54)$$

$$u = 0 \quad \text{on } \partial D \times (0, T), \quad (2.55)$$

$$u(\cdot, 0) = u_0 \quad \text{in } D, \quad (2.56)$$

$$q(\cdot, 0, \cdot) = q_0 \quad \text{in } D \times \Omega, \quad (2.57)$$

where  $q_0$  satisfies

$$\mathbb{E}(q_0) = 0 \quad \text{and} \quad \mathbb{E}(q_0 q_0^T) = I. \quad (2.58)$$

Note that comparing to (2.14), (2.15) (2.19) and (2.20) the hat symbols have been omitted for clarity purpose. Also note that equations (2.54) and (2.57) are notations for

$$\begin{aligned} q(x, t, \omega) - q_0(\omega) \\ = \int_0^t \left( \nabla u(x, s) q(x, s, \omega) - \frac{1}{2\lambda} q(x, s, \omega) \right) ds + \frac{1}{\sqrt{\lambda}} B(t, \omega), \end{aligned}$$

where  $(x, t, \omega) \in D \times [0, T] \times \Omega$ .

When  $D$  is of class  $\mathcal{C}^2$ , the implicit function theorem has been used in [16] to prove that the above problem admits a unique solution  $(u, p, q)$  satisfying

$$\begin{aligned} u &\in h^{1+\mu}([0, T]; L^r(D)) \cap h^\mu([0, T]; W^{2,r}(D)) \\ p &\in h^\mu([0, T]; W^{1,r}(D)) \\ q &\in L^\gamma(\Omega; h^\mu([0, T]; W^{1,r}(D))) \end{aligned} \quad (2.59)$$

with  $r > d$ ,  $0 < \mu < 1/2$  and  $\gamma \geq 2$ , for any data  $f$ ,  $u_0$ , small enough in appropriate spaces. Note that this regularity implies that the trajectories  $(x, t) \rightarrow q(x, t, \omega)$  are continuous, for almost each event  $\omega$ .

We now consider the finite element discretization in space. First, we assume that the existence result presented hereabove still holds when  $D$  is a convex polygon in  $\mathbb{R}^2$ . For any  $h > 0$ , let  $\mathcal{T}_h$  be a decomposition of  $D$  into triangles  $K$  with diameter  $h_K$  less than  $h$ , regular in the sense of [34]. We consider the finite element spaces  $V_h$ ,  $Q_h$  and  $R_h$  corresponding to continuous, piecewise linear velocity, pressure and dumbbells elongations. We denote  $i_h$  the  $L^2(D)$  projection onto  $V_h$ ,  $Q_h$  or  $R_h$  and introduce the following stabilized finite element

discretization in space of (2.52)-(2.57). Given  $f, u_0, q_0$  find

$$(u_h, p_h, q_h) : (0, T) \times \Omega \rightarrow V_h \times Q_h \times R_h,$$

$$(t, \omega) \rightarrow (u_h(t), p_h(t), q_h(t, \omega)),$$

such that  $u_h(0) = i_h u_0$ ,  $q_h(0, \omega) = q_0(\omega)$  and such that the following weak formulation holds in  $(0, T) \times \Omega$  :

$$\begin{aligned} & \rho \left( \frac{\partial u_h}{\partial t}, v_h \right)_D + 2\eta_s \left( \epsilon(u_h), \epsilon(v_h) \right)_D - \left( p_h, \operatorname{div} v_h \right)_D \\ & + \frac{\eta_p}{\lambda} \left( \mathbb{E}(q_h(q_h)^T) - I, \epsilon(v_h) \right)_D - \left( f, v_h \right)_D \\ & + \left( \operatorname{div} u_h, s_h \right)_D + \sum_{K \in T_h} \frac{\alpha h_K^2}{2\eta_p} \left( \nabla p_h, \nabla s_h \right)_K \\ & + (q_h(t), r_h)_D - (q_0, r_h)_D + \int_0^t \left( \frac{1}{2\lambda} q_h(k) - \nabla u_h(k) q_h(k), r_h \right)_D dk \\ & - \frac{1}{\sqrt{\lambda}} (B(t), r_h)_D = 0, \quad (2.60) \end{aligned}$$

for all  $(v_h, s_h, r_h) \in V_h \times Q_h \times R_h$ . Here  $\alpha > 0$  is a dimensionless stabilization parameter.

In order to avoid complications when considering stochastic processes with value in Banach spaces, the following decomposition is introduced

$$q = q^{eq} + q^d.$$

Here  $q^{eq} : [0, T] \times \Omega \rightarrow \mathbb{R}^d$  corresponds to physical equilibrium and is the so-called *Ornstein-Uhlenbeck* stochastic process satisfying

$$dq^{eq} = -\frac{1}{2\lambda} q^{eq} dt + \frac{1}{\sqrt{\lambda}} dB, \quad q^{eq}(0) = q_0, \quad (2.61)$$

while  $q^d : D \times [0, T] \times \Omega \rightarrow \mathbb{R}^d$  satisfies a deterministic differential equation with a stochastic forcing term

$$\frac{\partial q^d}{\partial t} + \frac{1}{2\lambda} q^d - (\nabla u) q^d = (\nabla u) q^{eq}, \quad q^d(0) = 0. \quad (2.62)$$

Then, using the fact that

$$\mathbb{E}(q^{eq}(s) q^{eq}(t)^T) = e^{-\frac{|t-s|}{2\lambda}} I, \quad s, t \in [0, T], \quad (2.63)$$

the momentum equation (2.52) writes :

$$\begin{aligned} & \rho \frac{\partial u}{\partial t} - 2\eta_s \operatorname{div} \epsilon(u) + \nabla p \\ & - \frac{\eta_p}{\lambda} \operatorname{div} \left( \mathbb{E}(q^d(q^d)^T + q^d(q^{eq})^T + q^{eq}(q^d)^T) \right) = f. \quad (2.64) \end{aligned}$$

As for the continuous problem, we use the decomposition

$$q_h = q^{eq} + q_h^d,$$

thus we are finally looking for  $(u_h, p_h, q_h^d)$  such that

$$\begin{aligned} & \left( \frac{\partial u_h}{\partial t}, v_h \right)_D + 2\eta_s \left( \epsilon(u_h), \epsilon(v_h) \right)_D - \left( p_h, \operatorname{div} v_h \right)_D \\ & + \frac{\eta_p}{\lambda} \mathbb{E}(q_h^d(q_h^d)^T + q_h^d(q^{eq})^T + q^{eq}(q_h^d)^T, \epsilon(v_h))_D - \left( f, v_h \right)_D \\ & + \left( \operatorname{div} u_h, s_h \right)_D + \sum_{K \in \mathcal{T}_h} \frac{\alpha h_K^2}{2\eta_p} (\nabla p_h, \nabla s_h)_K \\ & + (q_h^d(t), r_h)_D + \int_0^t \left( \frac{1}{2\lambda} q_h^d(k) - \nabla u_h(k)(q^{eq}(k) + q_h^d(k)), r_h \right)_D dk \\ & - \frac{1}{\sqrt{\lambda}} (B(t), r_h)_D dk = 0 \quad (2.65) \end{aligned}$$

for all  $(v_h, s_h, r_h) \in V_h \times Q_h \times R_h$ .

As in the previous subsection we write the above nonlinear problem as an abstract fixed point problem. Given  $y = (f, u_0) \in Y$ , find  $x_h = (u_h, q_h^d) \in X_h$  such that

$$x_h = \mathsf{T}_h(y, S_1(x_h), S_2(x_h)). \quad (2.66)$$

Here  $Y$  is the functional space for the data  $(f, u_0)$  (see [15] for details), and

$$X_h = L^2(0, T; V_h) \times L^2(\Omega; L^\infty(0, T; R_h)),$$

provided with the norm  $\|\cdot\|_{X_h}$  defined for all  $x_h = (u_h, q_h) \in X_h$  by

$$\|x_h\|_{X_h}^2 = 2\eta_s \int_0^T \|\epsilon(u_h(t))\|_{L^2(D)}^2 dt + \int_\Omega \sup_{t \in [0, T]} \|q_h(\omega, t)\|_{L^2(D)}^2 d\mathcal{P}(\omega).$$

Also, the operators  $S_1$  and  $S_2$  are defined by

$$S_1(x_h) = \mathbb{E}\left(q_h^d(q_h^d)^T\right) \quad \text{and} \quad S_2(x_h) = \nabla u_h q_h^d,$$

while the linear operator  $\mathsf{T}_h$  is defined by

$$\begin{aligned} \mathsf{T}_h : Y \times L^2(0, T; L^2(D)) \times L^2(\Omega; L^2(0, T; L^2(D))) & \rightarrow X_h \\ (f_1, u_0, f_2, w) & \rightarrow \mathsf{T}_h(f_1, u_0, f_2, w) = (\tilde{u}_h, \tilde{q}_h^d) \in X_h, \end{aligned}$$

where for  $(t, \omega) \in (0, T) \times \Omega$

$$(\tilde{u}_h, \tilde{p}_h, \tilde{q}_h^d) : (t, \omega) \rightarrow (\tilde{u}_h(t), \tilde{p}_h(t), \tilde{q}_h^d(t, \omega)) \in V_h \times Q_h \times R_h$$

satisfies  $\tilde{u}_h(0) = i_h u_0$  and

$$\begin{aligned} & \rho \left( \frac{\partial \tilde{u}_h}{\partial t}, v_h \right)_D + 2\eta_s \left( \epsilon(\tilde{u}_h), \epsilon(v_h) \right)_D - \left( \tilde{p}_h, \operatorname{div} v_h \right)_D \\ & + \frac{\eta_p}{\lambda} \left( \mathbb{E}(\tilde{q}_h^d(q^{eq})^T + q^{eq}(\tilde{q}_h^d)^T) + f_2, \epsilon(v_h) \right)_D - \left( f_1, v_h \right)_D \\ & + \left( \operatorname{div} \tilde{u}_h, s_h \right)_D + \sum_{K \in T_h} \frac{\alpha h_K^2}{2\eta_p} \left( \nabla \tilde{p}_h, \nabla s_h \right)_K \\ & (\tilde{q}_h^d(t), r_h)_D + \int_0^t \left( \frac{1}{2\lambda} \tilde{q}_h^d(k) - \nabla \tilde{u}_h(k) q^{eq}(k) - w, r_h \right)_D dk = 0, \end{aligned} \quad (2.67)$$

for all  $(v_h, s_h, r_h) \in V_h \times Q_h \times R_h$ , a.e. in  $(0, T)$  and a.e. in  $\Omega$ .

In [15], it is proved that (2.67) has a unique solution converging to that of (2.64) (2.62). As in the previous subsection (2.66) is rewritten as the following nonlinear problem : given  $y = (f, u_0) \in Y$ , find  $x_h = (u_h, q_h^d) \in X_h$  such that

$$F_h(y, x_h) = 0, \quad (2.68)$$

where  $F_h : Y \times X_h \rightarrow X_h$  is defined by

$$F_h(y, x_h) = x_h - \mathbf{T}_h(y, S_1(x_h), S_2(x_h)). \quad (2.69)$$

The abstract Theorem 2.1 of [29] can be then used in order to prove existence and convergence of a solution to (2.50). The mapping  $F_h : Y \times X_h \rightarrow X_h$  is  $C^1$ . Moreover, the scheme is consistent,  $D_x F_h$  has bounded inverse at  $i_h x$  and  $D_x F_h$  is locally Lipschitz at  $i_h x$ . Here  $i_h$  is the  $L^2(D)$  projection onto the finite element space  $X_h$  and  $x = (u, q^d)$  is the solution of the continuous problem (2.62) (2.64), with regularity (2.59). Therefore, applying Theorem 2.1 of [29], existence of a semi-discrete solution  $x_h$  can be proved in the neighbourhood of  $i_h x$  provided the data  $y$  is small enough in  $Y$ . Moreover, optimal error estimates hold for  $\|x - x_h\|_{X_h}$  that is :

$$\|u - u_h\|_{L^2(0,T;H^1(D))} + \|q^d - q_h^d\|_{L^2(\Omega; L^\infty(0,T; L^2(D)))} = O(h).$$

Note that the convergence result obtained here ensures the convergence of almost all trajectories. Also, a posteriori error estimates can be derived, we refer to [15] for details.



## Chapter 3

# Numerical Simulation of Viscoelastic Flows with Complex Free Surfaces

### 3.1 Space Discretization : Structured Cells and Finite Elements

We now come back to the splitting scheme described in sect. 2.2.1 to solve the free surface Oldroyd-B model. Recall that during the prediction step, three advection problems have to be solved which leads to formula (2.10)-(2.12), whereas during the correction step, the Oldroyd-B problem without convection (2.14)-(2.16) has to be solved.

Two distinct grids are used to solve the prediction and correction steps, see Fig. 3.1. Since the shape of the cavity  $\Lambda$  can be complex (this is for instance the case in mold filling or extrusion processes), finite element techniques are well suited for solving (2.14)-(2.16) using an unstructured mesh. On the other hand, a structured grid of cubic cells is used to implement (2.10)-(2.12). The reasons for using a structured grid is the following. Firstly, the method of characteristics can be easily implemented on structured grids. Secondly, the size of the cells can be tuned in order to control numerical diffusion when projecting (2.10)-(2.12) on the structured grid. Numerical experiments reported in [103, 104, 28] have shown that choosing the cells spacing three to five times smaller than the mesh spacing is a good trade-off between numerical diffusion and computational cost or memory storage.

We also refer to [138] for similar numerical simulations using finite difference methods.

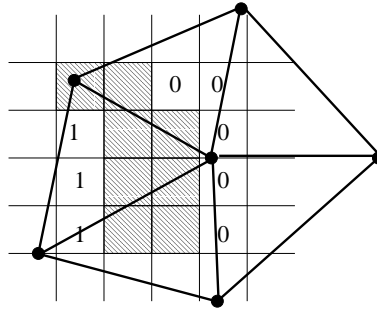


Figure 3.1: Two grids are used for the computations. In order to reduce numerical diffusion and to simplify the implementation, the volume fraction of liquid is computed on a structured grid of small cells. The velocity, pressure and extra-stress are computed on an unstructured finite element mesh with larger size. The symbol 1 (resp. 0) denotes a cell completely filled (resp. empty). The cells which are partially filled are shaded. The goal is to reduce the width of the partially filled region to a value smaller than the finite element spacing.

### 3.1.1 Advection Step : Structured Grid of Cubic Cells

The implementation of (2.10)-(2.12) is now discussed. Assume that the grid is made out of cubic cells  $C_{ijk}$  of size  $h$ . Let  $\varphi_{ijk}^{n-1}$ ,  $u_{ijk}^{n-1}$  and  $\sigma_{ijk}^{n-1}$  be the approximate value of  $\varphi$ ,  $u$  and  $\sigma$  at center of cell number  $(ijk)$  and time  $t^{n-1}$ . According to (2.10)-(2.12), the advection step on cell number  $(ijk)$  consists in advecting  $\varphi_{ijk}^{n-1}$ ,  $u_{ijk}^{n-1}$  and  $\sigma_{ijk}^{n-1}$  by  $\Delta t^n u_{ijk}^{n-1}$  and then projecting the values onto the structured grid. An example of cell advection and projection is presented in Fig. 3.2 in two space dimensions.

This advection algorithm is unconditionally stable with respect to the CFL condition - velocity times the time step divided by the cells spacing  $h$  - and  $O(\Delta t + h^2/\Delta t)$  convergent, according to the theoretical results available for the characteristics-Galerkin method [118, 119, 120]. However, this algorithm has two drawbacks. Indeed, numerical diffusion is introduced when projecting the values of the advected cells on the grid (recall that the volume fraction of liquid is discontinuous across the interface). Moreover, if the time step is too large, two cells may arrive at the same place, producing numerical (artificial) compression.

In order to enhance the quality of the volume fraction of liquid, two post-processing procedures have been implemented. We refer to [103, 104, 26] for a description in two and three space dimensions. The first procedure reduces numerical diffusion and is a simplified implementation of the SLIC (Simple Linear Interface Calculation) algorithm [33, 110, 134], see Figs. 3.3 and 3.4 for a simple example. In the SLIC procedure, if a cell is partially filled with liquid, then the volume fraction of liquid is condensed along the cells faces,

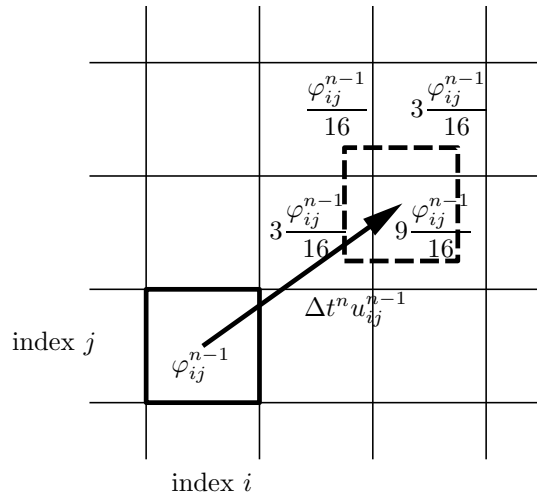


Figure 3.2: An example of two dimensional advection of  $\varphi_{ij}^{n-1}$  by  $\Delta t^n u_{ij}^{n-1}$ , and projection on the grid. The advected cell is represented by the dashed lines. The four cells containing the advected cell receive a fraction of  $\varphi_{ij}^{n-1}$ , according to the position of the advected cell. In this example, the new values of the volume fraction of liquid  $\varphi^n$  are updated as follows :  $\varphi_{i+1,j+1}^n = \varphi_{i+1,j+1}^n + 3/16\varphi_{ij}^{n-1}$ ;  $\varphi_{i+2,j+1}^n = \varphi_{i+2,j+1}^n + 9/16\varphi_{ij}^{n-1}$ ;  $\varphi_{i+1,j+2}^n = \varphi_{i+1,j+2}^n + 1/16\varphi_{ij}^{n-1}$ ;  $\varphi_{i+2,j+2}^n = \varphi_{i+2,j+2}^n + 3/16\varphi_{ij}^{n-1}$ .

edges or corners (see Fig. 3.5), according to the volume fraction of liquid of the neighbouring cells (see Fig. 3.6).

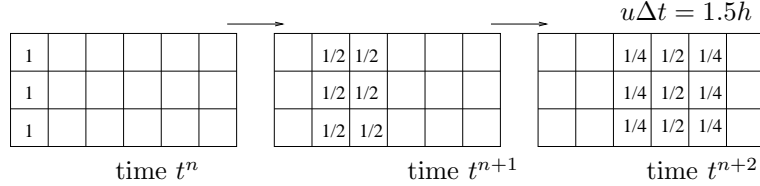


Figure 3.3: Numerical diffusion during the advection step. At time  $t^n$ , the cells have volume fraction of liquid one or zero. The velocity  $u$  is horizontal, the time step  $\Delta t$  is chosen so that  $u\Delta t = 1.5h$  where  $h$  is the cells spacing.

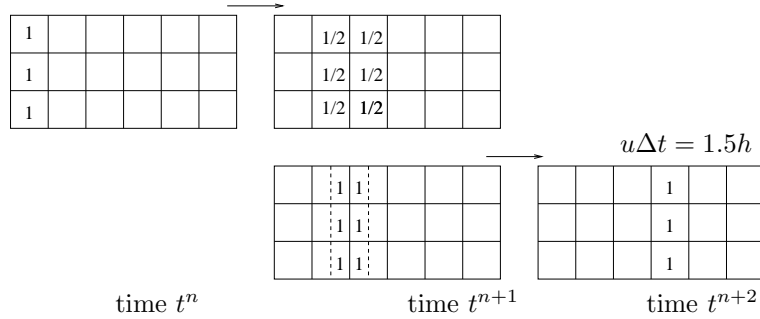


Figure 3.4: Reducing numerical diffusion using the SLIC algorithm. Before advecting a cell partially filled with liquid, the volume fraction of liquid is condensed along the cells boundaries, according to the neighbouring cells.

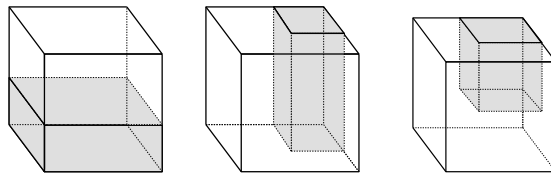


Figure 3.5: SLIC algorithm. If the cell is partially filled with liquid, the liquid is pushed along a face, an edge, or a vertex of the cell, according to the neighbours volume fraction of liquid.

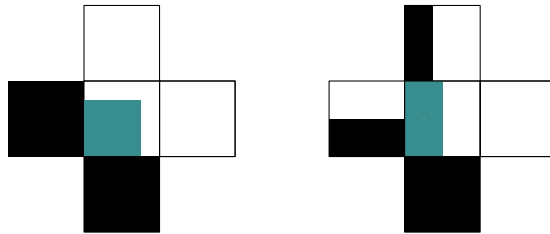


Figure 3.6: SLIC algorithm. The volume fraction of liquid in a cell partially filled with liquid is pushed according to the volume fraction of liquid of the neighbouring cells. Two examples are proposed. Left: the left and bottom neighbouring cells are full of liquid, the right and top neighbouring cells are empty, the liquid is pushed at the bottom left corner of the cell. Right: the bottom neighbouring cell is full of liquid, the right neighbouring cell is empty, the other two neighbouring cells are partially filled with liquid, the volume fraction of liquid is pushed along the left side of the cell.

The second procedure removes artificial compression (that is values of the volume fraction of liquid greater than one), which may happen when the volume fraction of liquid advected in two cells arrive at the same place, see Fig. 3.7. The aim of this procedure is to produce new values  $\varphi_{ijk}^n$  which are between zero and one and is as follows. At each time step, all the cells having values  $\varphi_{ijk}^n$  greater than one (strictly) or between zero and one (strictly) are sorted according to their values  $\varphi_{ijk}^n$ . This can be done in an efficient way using quick sort algorithms. The cells having values  $\varphi_{ijk}^n$  greater than one are called the dealer cells, whereas the cells having values  $\varphi_{ijk}^n$  between zero and one are called the receiver cells. The second procedure then consists in moving the fraction of liquid in excess in the dealer cells to the receiver cells, see [103, 104] for details.

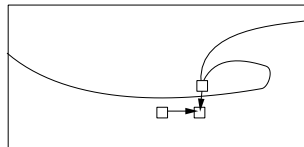


Figure 3.7: An example of numerical (artificial) compression.

Validation of these procedures using standard two dimensional test cases taken from [2, 127] have been performed in [26]. Translation, rotation and stretching of a circular region of fluid are shown in Fig. 3.8. For more details we refer to Sect. 5.1 of [26].

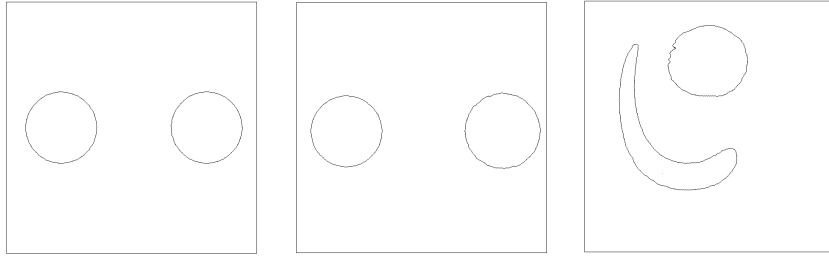


Figure 3.8: Validation of the advection step. Left: Translation of a circular region of liquid, the interface is shown at initial and final time. Middle: Rotation of a circular region of liquid, the interface is shown at initial and final time. Right: Single vortex test case, the interface is shown at time  $t = 1$  (maximal deformation) and  $t = 2$  s (return to initial circular shape).

In a number of industrial applications, the shape of the cavity containing the liquid is complex. Therefore, a special data structure has been implemented in order to reduce the memory requirements used to store the cell data. An example is proposed in Fig. 3.9. The cavity containing the liquid is meshed into tetrahedrons. Without any particular cells data structure, a great number of cells would be stored in the memory without ever being used. The data structure makes use of three hierarchical levels to define the cells. At the coarsest level, the cavity is meshed into windows which can be glued together. Each window is then subdivided into blocks. Finally, a block is cut into smaller cubes, namely the cells  $(ijk)$ . When a block is free of liquid ( $\varphi = 0$ ), it is switched off, that is to say the memory corresponding to the cells is not allocated. When liquid enters a block, the block is switched on, that is to say the memory corresponding to the cells is allocated.

Once values  $\varphi_{ijk}^n$ ,  $u_{ijk}^{n-\frac{1}{2}}$  and  $\sigma_{ijk}^{n-\frac{1}{2}}$  have been computed on the cells  $(ijk)$ , values are interpolated at the vertices  $P$  of the finite element mesh. More precisely, the volume fraction of liquid at vertex  $P$  is computed by considering all the cells  $(ijk)$  contained in the triangles  $K$  containing vertex  $P$ , see Fig. 3.10, using the following formula :

$$\varphi^n(P) = \frac{\sum_{\substack{K \\ P \in K}} \sum_{(ijk) \subset K} \phi_P(x_{ijk}) \varphi_{ijk}^n}{\sum_{\substack{K \\ P \in K}} \sum_{(ijk) \subset K} \phi_P(x_{ijk})}. \quad (3.1)$$

Here  $x_{ijk}$  denotes the center of cell  $(ijk)$  and  $\phi_P$  is the finite element basis function attached to vertex  $P$ . Similar formula hold for the velocity and extra-stress. Then, the liquid region is defined as follows. An element (tetrahedron) of the mesh is said to be liquid if (at least) one of its vertices has a volume fraction of liquid  $\varphi^n > 0.5$ , see Fig. 3.11. The computational domain  $D^n$  used

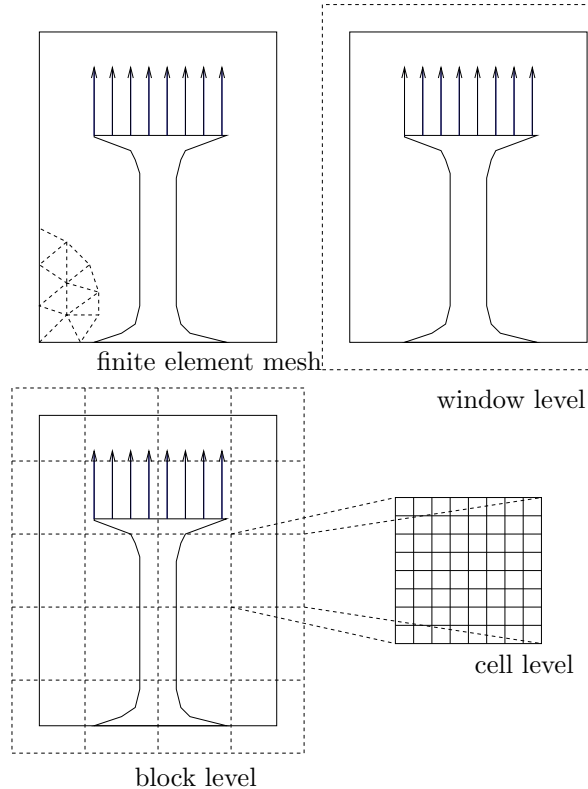


Figure 3.9: The hierarchical window-block-cell data structure used to implement cells advection in the framework of the 2D filament stretching.

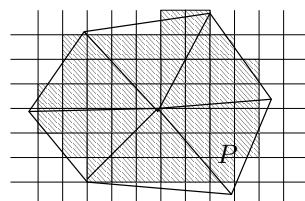


Figure 3.10: Interpolation of the volume fraction of liquid from the structured cells to the unstructured finite element mesh. The volume fraction of liquid at vertex  $P$  depends on the volume fraction of liquid in the shaded cells.

for solving (1.2)-(1.8) is then defined to be the union of all liquid elements. At this point, we would like to stress that the values of the volume fraction of liquid on the unstructured finite element mesh are only used in order to define the liquid region. Again, advection of the volume fraction of liquid only occurs on the structured cells, and not on the unstructured finite element mesh. Also, the volume constraint is not directly enforced in the numerical model. However, if numerical diffusion of the volume fraction of liquid is small, then the volume constraint will be satisfied. This is precisely the goal of the two post-processing procedures that have been added. In all the computations, we have observed that the (numerical) diffusion layer of the volume fraction of liquid ( $0 < \varphi < 1$ ) is of the order of one or two cells and that the volume constraint is satisfied up to 1%. In order to achieve this goal, the two post-processing procedures must be switched on and the cells spacing must be three to five times smaller than the mesh spacing.

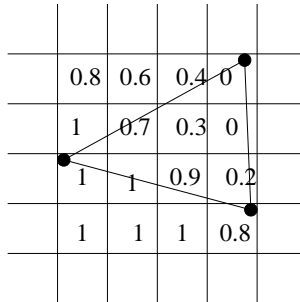


Figure 3.11: A two dimensional example of liquid element. The values of the volume fraction of liquid  $\varphi$  at the center of the cells are known. A value  $\varphi$  is then interpolated at the vertices of the finite element mesh. The displayed triangle has at least one vertex with value  $\varphi$  greater than 0.5. Therefore, the triangle is liquid and the velocity, the pressure and the extra-stress will be computed at the three vertices of the triangle.

### 3.1.2 Correction Step : Stokes and Oldroyd-B with Finite Elements

Let us now turn to the finite element techniques used for solving (2.14)-(2.16). Given the new liquid domain  $D^n$  (remember that  $D^n$  is the union of liquid elements belonging to the mesh), let  $V_h$ ,  $Q_h$  and  $M_h$  be the finite element subspaces of continuous, piecewise linear velocity, pressure and extra-stress defined on  $D^n$ . We follow sect. 2.3.2 and use an EVSS (Elastic Viscous Split Stress) formulation with continuous, piecewise linear stabilized finite elements. More precisely, given the predicted velocity  $u_h^{n-1/2} \in V_h$ , the extra-variable  $d_h^{n-1/2} \in M_h$  defined by

$$(d_h^{n-1/2}, e_h)_{D^n} = (\epsilon(u_h^{n-1/2}), e_h)_{D^n} \quad \forall e_h \in M_h,$$

is introduced for stability purposes. Solving this equation results in solving a diagonal linear system provided a mass lumping quadrature formula is used. Since the mass lumping quadrature formula is order two accurate in space, the global accuracy of the method is not affected. Once  $d_h^{n-1/2}$  is computed, the predicted extra-stress  $\sigma_h^{n-1/2}$  being known, the new velocity  $u_h^n \in V_h$  and pressure  $p_h^n \in Q_h$  are obtained by solving the following Stokes problem

$$\begin{aligned} & \frac{\rho}{\Delta t^n} (u_h^n, v_h)_{D^n} + 2(\eta_s + \eta_p) (\epsilon(u_h^n), \epsilon(v_h))_{D^n} - (p^n, \operatorname{div} v_h)_{D^n} \\ &= \frac{\rho}{\Delta t^n} (u_h^{n-1/2}, v_h)_{D^n} (2\eta_p d_h^{n-1/2} - \sigma^{n-1/2}, \epsilon(v_h))_{D^n} + (\rho g, v_h)_{D^n}, \\ & (\operatorname{div} u_h^n, q_h)_{D^n} + \sum_{K \subset D^n} \alpha_K \left( \frac{\rho}{\Delta t^n} u_h^n + \nabla p_h^n, \nabla q_h \right)_{D^n} \\ &= \sum_{K \subset D^n} \alpha_K \left( \frac{\rho}{\Delta t^n} u_h^{n-1/2} + \operatorname{div} \sigma_h^{n-1/2} + \rho g, \nabla q_h \right)_{D^n}, \end{aligned} \quad (3.2)$$

for all test functions  $v_h \in V_h$  and  $q_h \in Q_h$ . Here  $\alpha_K$  is the local stabilization coefficient defined by

$$\alpha_K = \begin{cases} \frac{|K|^{2/3}}{12(\eta_s + \eta_p)} & \text{if } Re_K \leq 3, \\ \frac{|K|^{2/3}}{4Re_K(\eta_s + \eta_p)} & \text{else,} \end{cases}$$

where, following [56], the local Reynolds number  $Re_K$  is defined by

$$Re_K = \frac{\rho |K|^{\frac{1}{3}} \|u_h^{n-1/2}\|_{L^\infty(K)}}{2(\eta_s + \eta_p)}.$$

Note that in (3.2) the corrected velocity  $u_h^n$  can be prescribed on the boundary of the cavity  $\Lambda$  whenever needed, see Fig. 1.5 for a discussion related to boundary conditions. Also note that the boundary condition (1.17) is implicitly contained in the above variational formulation. All the degrees of freedom corresponding to velocity and pressure are stored in a single matrix and the linear system is solved using the GMRES algorithm with a classical incomplete LU preconditioner and no restart.

It then remains to update the extra-stress  $\sigma_h^n \in M_h$  from Oldroyd-B constitutive equation :

$$\begin{aligned} \left( 1 + \frac{\lambda}{\Delta t^n} \right) (\sigma^n, \tau)_{D^n} &= \left( \frac{\lambda}{\Delta t^n} \sigma^{n-1/2} \right. \\ &\quad \left. + \lambda \nabla u_h^n \sigma^{n-1/2} + \lambda \sigma^{n-1/2} (\nabla u_h^n)^T + 2\eta_p (\epsilon(u_h^n), \tau) \right)_{D^n} \quad \forall \tau \in M_h. \end{aligned}$$

Here  $\sigma_h^n$  must be prescribed at the inflow boundary, if there is one, see Fig. 1.5. Again, this equation results in solving a diagonal linear system whenever a mass lumping quadrature formula is used.

Finally, once the new velocity  $u_h^n$  and extra-stress  $\sigma_h^n$  are computed at the vertices of the finite element mesh, values are interpolated at the center of the cells  $(ijk)$ :

$$u_{ijk}^n = \sum_P \phi_P(x_{ijk}) u_P^n, \quad (3.3)$$

where  $P$  denotes a mesh vertex,  $x_{ijk}$  denotes the center of cell  $(ijk)$ ,  $\phi_P$  denotes the finite element basis function corresponding to vertex  $P$  and  $u_P^n$  is the velocity at vertex  $P$ . A similar formula is used for the extra-stress  $\sigma_{ijk}^n$ . Please note that the volume fraction of liquid is not interpolated from the finite element mesh to the cells. Indeed, the volume fraction of liquid is only computed on the structured cells. It is interpolated on the unstructured finite element mesh only in order to define the liquid region after the prediction step, see the end of Sect. 4.1 above.

### 3.1.3 Implementations Details

The memory storage is the following. For each cubic cell, the volume fraction of liquid, the velocity and the extra-stress must be stored in order to implement (2.10)-(2.12), therefore  $1 + 3 + 6 = 10$  values. For each vertex of the finite element mesh, the velocity, the pressure, the extra-stress and the EVSS field  $d_h^{n-1/2}$  must be stored, therefore  $3 + 1 + 6 + 6 = 16$  values. The code is written in the C++ programming language and the finite element data structure is classical. The data structure of the cells is as follows. Each cell is labelled by indices  $(ijk)$  within a block. Also, each block is labelled by indices  $(ijk)$  within a window, see Fig. 3.9.

In order to perform efficient interpolation between the two grids (structured cells/unstructured finite elements), the following data structure is needed. In order to implement interpolation from the finite element mesh to the cells, eq. (3.3), the index of the finite element (tetrahedron) containing each cell is needed. Alternatively, in order to implement interpolation from the cells to the finite element mesh, eq. (3.1), the list of the cells contained in each finite element (tetrahedron) is required. This additional data structure is built at the beginning of each computation. It can be stored in case several computations are performed with the same grids. The additional CPU time required to build this data structure is small (less than 1%) compared to the total CPU time.

## 3.2 Extension to Mesoscopic Models

Computations with the FENE free surface algorithm presented in sect. 2.2.2 have been performed in [60] in two space dimensions and are not reported here. The use of variance reduction techniques is advocated, see for instance [20, 73].

### 3.3 Numerical Results

In this section, numerical results pertaining to Oldroyd-B three dimensional flows with complex free surfaces are presented. First, the method is validated on test cases for which an exact solution is available. Then, numerical simulations are proposed on two test cases involving flows with complex free surfaces, namely jet buckling and the stretching of a filament.

#### 3.3.1 Numerical Validation

##### Elongational Flow

At initial time, liquid at rest occupies a cylinder with radius  $R_0 = 0.0034\text{ m}$  and height  $L_0 = 0.0019\text{ m}$ . Then, the velocity field on the top and bottom sides of the cylinder is imposed to be

$$u(x, y, z, t) = \begin{pmatrix} -\frac{1}{2}\dot{\epsilon}_0 x \\ -\frac{1}{2}\dot{\epsilon}_0 y \\ \dot{\epsilon}_0 z \end{pmatrix},$$

with  $\dot{\epsilon}_0 = 4.68\text{ s}^{-1}$ , whereas (1.17) applies on the lateral sides. Since there is no inflow velocity, no boundary conditions have to be enforced for the extra-stress. A simple calculation shows that, for all time  $t$ , the above velocity field satisfies the momentum equations, that the extra-stress tensor is homogeneous, for instance

$$\sigma_{zz}(x, y, z, t) = \frac{2\eta_p\dot{\epsilon}_0}{1 - 2\dot{\epsilon}_0\lambda} \left(1 - e^{-(\frac{1}{\lambda} - 2\dot{\epsilon}_0)t}\right),$$

and that the liquid region remains a cylinder with radius  $R(t) = R_0 e^{-\frac{1}{2}\dot{\epsilon}_0 t}$ . Indeed, the trajectories of the fluid particles are defined by  $X'(t) = u(X(t), t)$  which yields

$$\begin{cases} X(t) = X(0)e^{-\frac{1}{2}\dot{\epsilon}_0 t} \\ Y(t) = Y(0)e^{-\frac{1}{2}\dot{\epsilon}_0 t} \\ Z(t) = Z(0)e^{\dot{\epsilon}_0 t} \end{cases}.$$

Two meshes are used for the computations. The computational domain is the block  $[-0.004\text{ m}, 0.004\text{ m}] \times [-0.004\text{ m}, 0.004\text{ m}] \times [0\text{ m}, 0.03\text{ m}]$  in the  $xyz$  directions. The 3D meshes are obtained by extruding the 2D meshes shown in Fig. 3.12, from  $z = 0$  to  $z = 0.03\text{ m}$ , and then cutting the prisms into tetrahedrons. The coarse (resp. fine) mesh has 62000 (resp. 462000) vertices and mesh size  $0.00035\text{ m}$  (resp.  $0.000175\text{ m}$ ). When using the coarse (resp. fine) mesh, the cell size is  $0.0001\text{ m}$  (resp.  $0.00005\text{ m}$ ). The time step was  $\Delta t = 0.01\text{ s}$  for the coarse mesh (resp.  $\Delta t = 0.005\text{ s}$  for the fine mesh) so that the CFL number of the cells - velocity times the time step divided by the cells spacing - equals 0.9 at time  $t = 0$  and 3.7 at time  $t = 0.3$ .

Numerical results corresponding to 0.05 % by weight Polystyrene (the parameter values are taken from [35],  $\rho = 1030\text{ kg/m}^3$ ,  $\eta_s = 9.15\text{ Pa.s}$ ,  $\eta_p = 25.8\text{ Pa.s}$ ,  $\lambda = 0.421\text{ s}$ , thus  $De = \lambda\dot{\epsilon}_0 = 1.97$ ) are reported in Fig. 3.13 and 3.14. Clearly

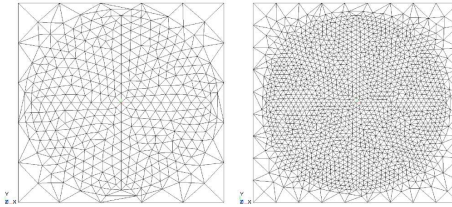


Figure 3.12: Elongational flow : 2D cut of the mesh at  $z = 0$ ; left : coarse mesh; right : fine mesh.

the computed velocity agrees perfectly with the exact velocity whereas the error for the extra-stress is within 10% on the fine grid. The fact that the velocity is more precise than the extra-stress is not surprising since the finite element method is expected to be of order two (in the  $L^2$  norm and in a fixed domain) for the velocity but only of order one for the extra-stress.

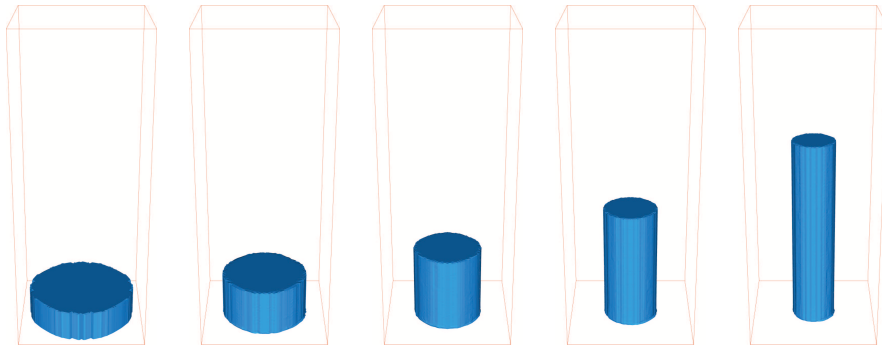


Figure 3.13: Elongational flow : shape of the liquid region (the volume corresponding to volume fraction of liquid  $\varphi > 0.5$  is shown); simulation at different times (from left to right):  $t = 0$  s,  $0.1$  s,  $0.2$  s,  $0.3$  s,  $0.4$  s.

### Filling of a Straight Pipe

Consider a rectangular pipe of dimensions  $[0, L_1] \times [0, L_2] \times [0, L_3]$  in the  $xyz$  directions, where  $L_1 = 4$  m,  $L_2 = 1$  m,  $L_3 = 0.3$  m. At the initial time, the pipe is empty. Then, fluid enters from the left side ( $x = 0$ ) with velocity and extra-stress given by

$$u(x, y, z, t) = \begin{pmatrix} u_x \\ 0 \\ 0 \end{pmatrix}, \quad \sigma(x, y, z, t) = \begin{pmatrix} \sigma_{xx} & \sigma_{xy} & 0 \\ \sigma_{xy} & 0 & 0 \\ 0 & 0 & 0 \end{pmatrix}, \quad (3.4)$$

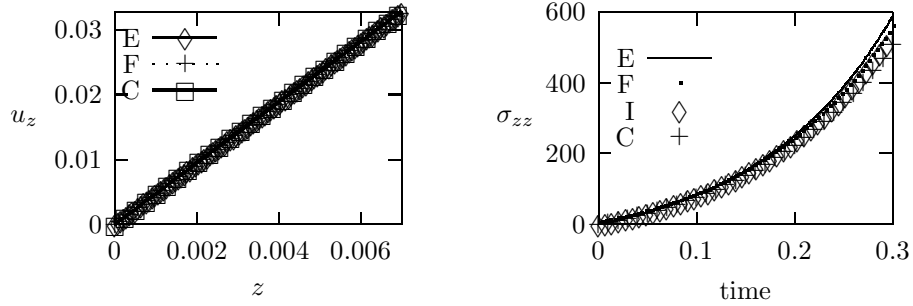


Figure 3.14: Elongational flow (E=Exact solution, F=Fine mesh, I= Intermediate mesh, C=Coarse mesh); left : vertical velocity  $u_z$  along the vertical axis  $Oz$  at final time  $t = 0.3$  s; right : extra-stress  $\sigma_{zz}$  at  $z = 0.0006$  m as a function of time.

with  $u_x(y) = 6y(L_2 - y)$ ,  $\sigma_{xx}(y) = 72\eta_s\lambda(2y - L_2)^2$  and  $\sigma_{xy}(y) = -6\eta_p(2y - L_2)$ . The boundary conditions are detailed in Fig. 3.15 and are the following. On the top and bottom sides ( $y = 0$  and  $y = L_2$ ), no-slip boundary conditions apply. On the front and rear sides ( $z = 0$  and  $z = L_3$ ), slip boundary conditions apply. On the right side ( $x = L_1$ ) the fluid is free to exit the pipe with zero vertical velocity. The parameter values are taken from [139] subsection 6.1 and are the following :  $\rho = 1 \text{ kg/m}^3$ ,  $\eta_s = \eta_p = 0.5 \text{ Pa.s}$ . Three finite element meshes are used in this subsection, see Table 3.1. for details. The cells spacing is five times smaller than the finite element mesh spacing.

We first consider the filling of the pipe, starting from an empty pipe. This experiment has been considered in [117, 139] and is sometimes called fountain flow. The imposed velocity and extra-stress profile at the inlet are those corresponding to Poiseuille flow, see (3.4). Following [59], after some time the shape of free surface should be close to a half circle. In Fig. 3.15, the velocity and the shape of the free surface is shown at several times. The mesh is the finest one and the time step is  $\Delta t = 0.03$  s, so that the CFL number of the cells - velocity times the time step divided by the cells spacing - equals 4.5. Away from the inlet, the position of the free surface is the same for both Newtonian and viscoelastic flows, see Fig. 3.16. As predicted theoretically [59], the shape is almost circular. Details of the fountain flow at the free surface is provided in Fig. 3.16.

Once totally filled with liquid, the velocity and extra-stress must satisfy (3.4) in the whole pipe. Convergence of the stationary solution is checked with  $\lambda = 1$  s, thus  $De = \lambda U/L_2 = 1$ , where  $U = 1 \text{ m/s}$  is the average velocity. In Fig. 3.17,  $\sigma_{xx}$ ,  $\sigma_{xy}$  and  $u_x$  are plotted along the vertical line  $x = L_1/2$ ,  $0 \leq y \leq L_2$ ,  $z = L_3/2$ . Convergence can be observed even though boundary layer effects are present, this being classical with low order finite elements. In Fig. 3.18, the error in the  $L^2$  norm of  $\sigma_{xx}$ ,  $\sigma_{xy}$  and  $u_x$  is plotted versus the mesh size. Clearly order one convergence rate is observed for the extra-stress,

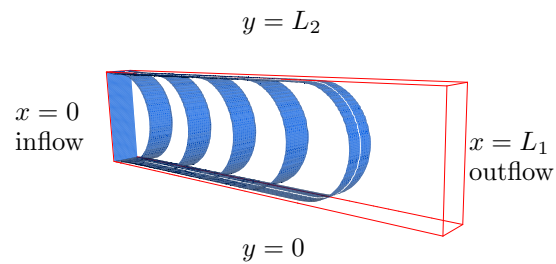


Figure 3.15: Filling of a pipe; notations and isovalue  $\varphi = 0.5$  for a Newtonian fluid at times  $t = 0, 0.6, 1.2, 1.8, 2.4, 3.0$  s.

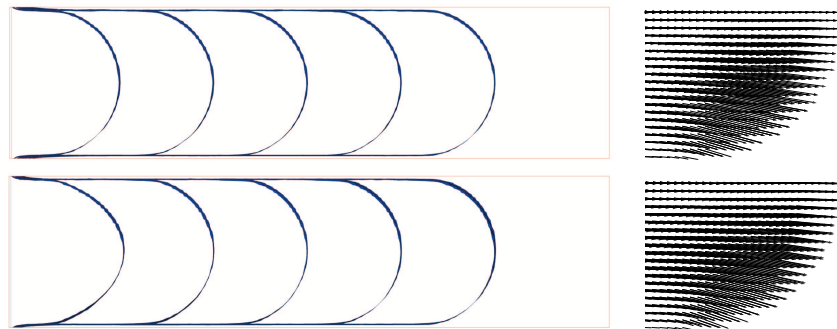


Figure 3.16: Filling of a pipe. Left : position of the free surface at time  $t = 0, 0.6, 1.2, 1.8, 2.4, 3.0$  s. Right : Velocity field close to the free surface at time  $t = 1.8$  s. Top : Newtonian flow. Bottom : viscoelastic flow ( $\lambda = 5$  s thus  $De = 5$ ).

order two for the velocity, this being consistent with theoretical predictions on simplified problems.

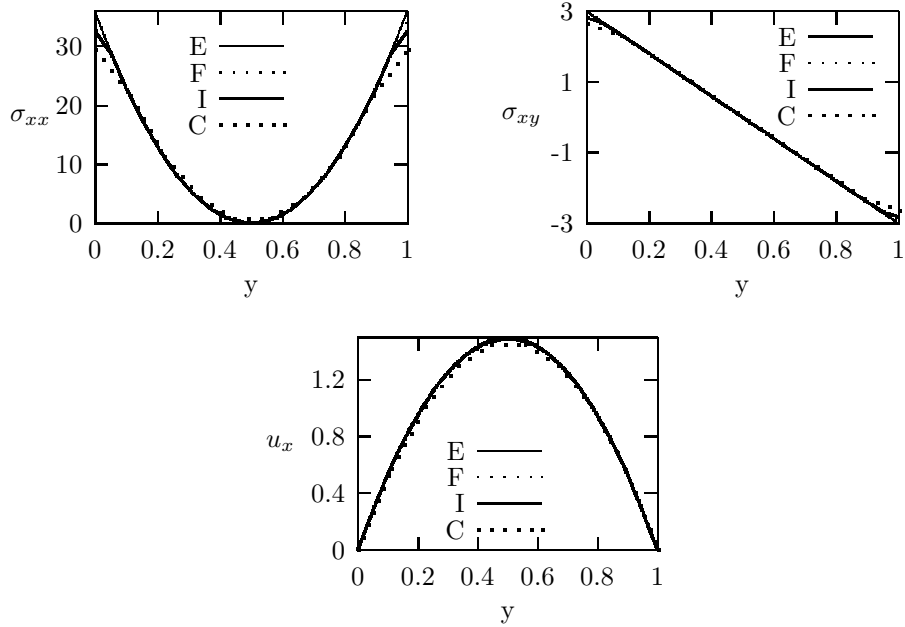


Figure 3.17: Filling of a pipe; In all the plots E=Exact solution, F=Fine mesh, I=Intermediate mesh and C=Coarse mesh; top left:  $\sigma_{xx} = 72\eta_s\lambda(2y-L_2)^2$  along the vertical line  $x = L_1/2$ ,  $0 \leq y \leq L_2$ ,  $z = L_3/2$ ; middle :  $\sigma_{xy} = -6\eta_p(2y-L_2)$ , bottom : horizontal velocity  $u_x = 6y(L_2-y)$ .

Mesh	Subdivisions (radius × height)	Vertices	Tetrahedrons
coarse	$40 \times 10 \times 3$	1804	7200
intermediate	$80 \times 20 \times 6$	11900	57600
fine	$160 \times 40 \times 12$	85813	460800

Table 3.1: Filling of a pipe; the three mesh used to check convergence.

### 3.3.2 Jet Buckling

The transient flow of a 3D jet injected into a parallelepiped cavity is now reproduced. The cavity is a parallelepiped of width 0.05 m, depth 0.05 m and height 0.1 m, the diameter of the jet being  $D = 0.005$  m. Liquid enters from the top of the cavity with vertical velocity  $U = 0.5$  m/s. The fluid parameters are

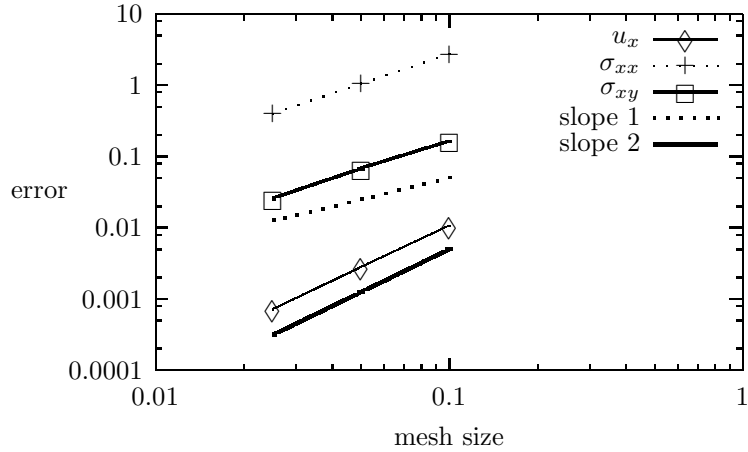


Figure 3.18: Filling of a pipe; error in the  $L^2$  norm with respect to the mesh size.

$\rho = 1030 \text{ kg/m}^3$ , in the Newtonian case the viscosity is  $\eta_s + \eta_p = 10.3 \text{ Pa.s}$  and  $\lambda = 0 \text{ s}$ , in the viscoelastic case, the viscosities are  $\eta_s = 1.03$ ,  $\eta_p = 9.27 \text{ Pa.s}$ , and the relaxation time  $\lambda = 1 \text{ s}$  so that  $De := \lambda U/D = 100$ . The finite element mesh has 503171 vertices and 2918760 tetrahedrons. The cells size is  $0.0002 \text{ m}$  and the time step is  $0.001 \text{ s}$  thus the CFL number of the cells - velocity times the time step divided by the cells spacing - is 2.5. The shape of the jet is shown in Fig. 3.19-3.20 for Newtonian and viscoelastic flows. This computation took 64 hours on a AMD opteron CPU with 8Gb memory.

In [140], Tomé and McKee provided an empirical threshold on the Reynolds number for a Newtonian jet to buckle. Our experiments indicates that this relation does not hold for viscoelastic flow and that the Weissenberg number should be taken into account, see [19].

### 3.3.3 Filament Stretching

The flow of an Oldroyd-B fluid contained between two parallel coaxial circular disks with radius  $R_0 = 0.003 \text{ m}$  is considered. At the initial time, the distance between the two end-plates is  $L_0 = 0.0019 \text{ m}$  and the liquid is at rest. Then, the top end-plate is moved vertically with velocity  $L_0 \dot{\epsilon}_0 e^{\dot{\epsilon}_0 t}$ . The model data ( $\rho$ ,  $\eta_s$ ,  $\eta_p$ ,  $\lambda$ ,  $\dot{\epsilon}_0$ ) are those of subsection 5.1. The fine mesh of subsection 5.1 was used with an initial time step  $\Delta t^0 = 0.005 \text{ s}$ , thus the initial CFL number of the cells - velocity times the time step divided by the cells spacing - is close to one, the time step at time  $t^n$  being such that the distance of the moving end-plate between two time steps is constant, that is

$$\Delta t^n = \Delta t^{n-1} e^{-\dot{\epsilon}_0 \Delta t^{n-1}}.$$

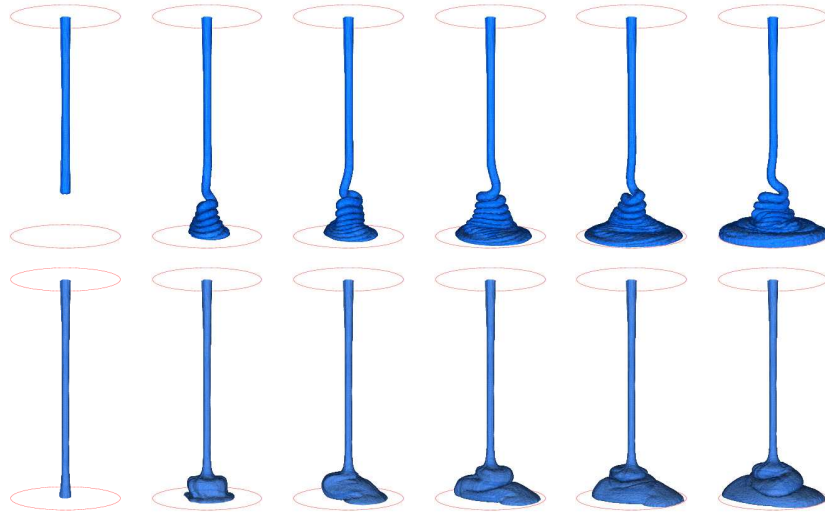


Figure 3.19: Jet buckling in a thick cavity. Shape of the jet at time  $t = 0.125$  s (col. 1),  $t = 0.45$  s (col. 2),  $t = 0.6$  s (col. 3),  $t = 0.9$  s (col. 4),  $t = 1.15$  s (col. 5),  $t = 1.6$  s (col. 6), Newtonian fluid (row 1), viscoelastic fluid  $De = 100$  (row 2).

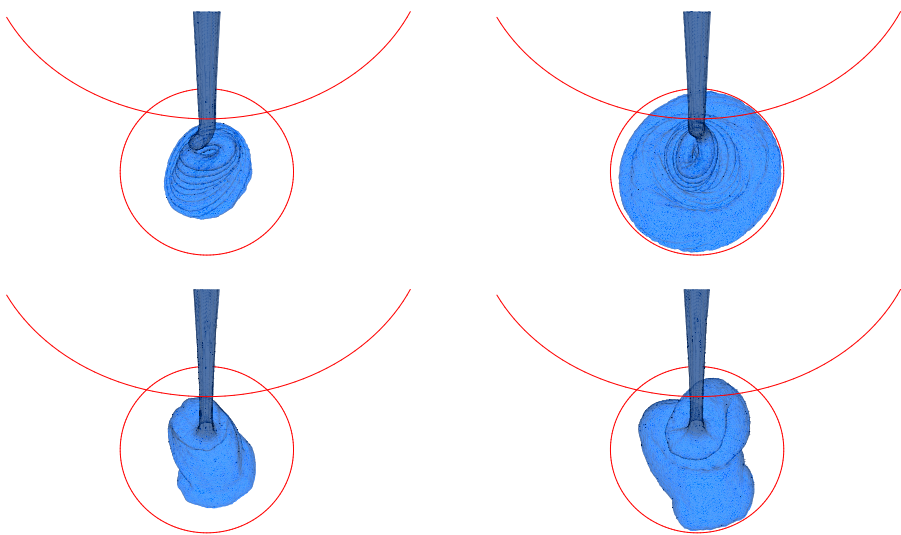


Figure 3.20: Jet buckling in a thick cavity. View from the top. Shape of the jet at time  $t = 0.6$  s (col. 1),  $t = 1.15$  s (col. 2), Newtonian fluid (row 1), viscoelastic fluid  $De = 100$  (row 2).

Therefore, the CFL number remains constant throughout the simulation. The shape of the liquid region at time  $t = 0.5$  s is represented in Fig. 3.21, for both Newtonian and non-Newtonian computations. As reported in [145], the 'necking' phenomena occurring in the central part of the liquid for Newtonian fluids is not observed for viscoelastic fluids, due to strain hardening. This calculation requires 2 hours (resp. 24 hours) on the coarse mesh (resp. fine mesh) using a single user Pentium 4 CPU 2.8 Ghz, with 2Gb memory, under the Linux operating system. Most of the time is spent in solving the associated Stokes problem. The memory usage is 200 Mb for the coarse mesh, resp. 1.6 Gb for the fine mesh.

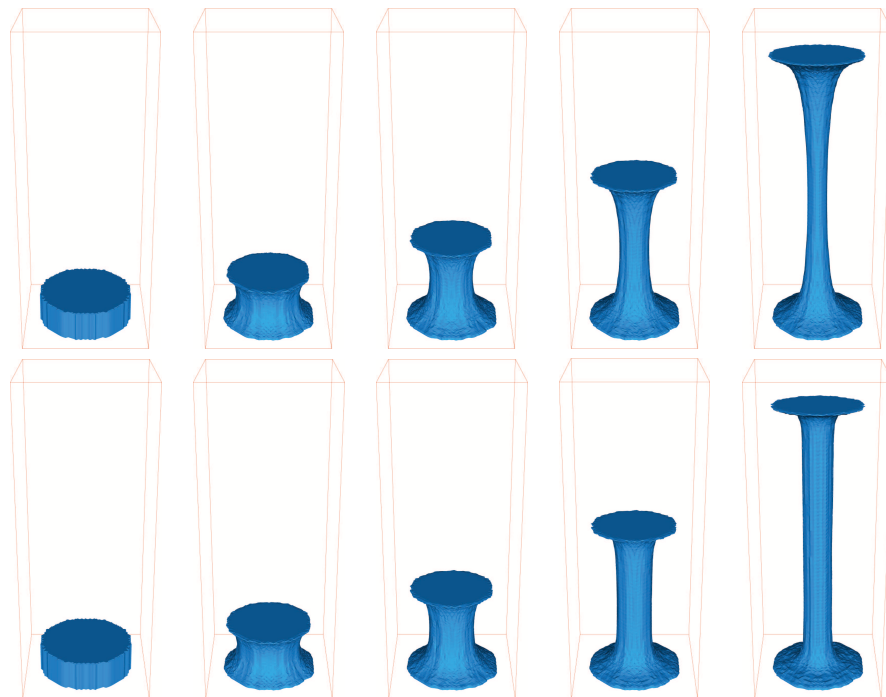


Figure 3.21: Filament stretching. Aspect ratio  $L_0/R_0 = 19/30$ . The Hencky strains  $\epsilon := \dot{\epsilon}_0 t$  are: (column 1) 0; (column 2) 0.57; (column 3) 1.12; (column 4) 2.25; (column 5) 4.49; (top row) Newtonian fluid; (bottom row) Viscoelastic fluid with  $\lambda = 0.421$  s ( $We = 1.97$ ).

We now show that our numerical model is capable to reproduce fingering instabilities reported in [121, 5, 105, 40] for non-Newtonian flows. Following Sect. 4.4 in [105], we take an aspect ratio  $L_0/R_0 = 1/20$  ( $R_0 = 0.003$  m,  $L_0 = 0.00015$  m), so that the Weissenberg number  $We = DeR_0^2/L_0^2$  is large. The finite element mesh has 50 vertices along the radius and 25 vertices along the height, thus the mesh size is 0.00006 m. The cells size is 0.00001 m and

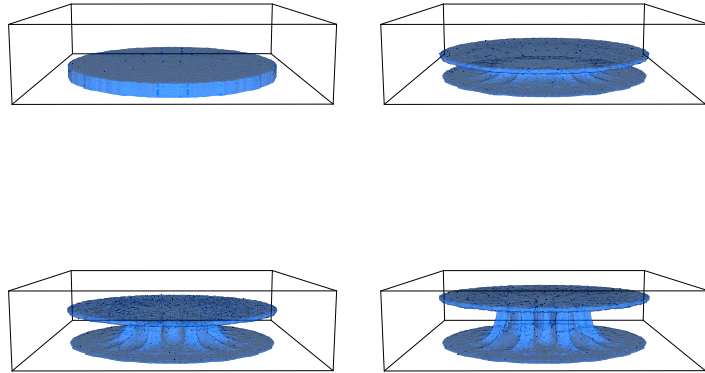


Figure 3.22: Filament stretching,  $\lambda = 0.421\text{ s}$  ( $We = 1.97$ ), aspect ratio  $L_0/R_0 = 1/20$ . Shape of the liquid region at time: (top left)  $t = 0\text{ s}$ , (top right)  $t = 0.33\text{ s}$ , (bottom left)  $t = 0.66\text{ s}$ , (bottom right)  $t = 1\text{ s}$ .

the initial time step is  $\Delta t^0 = 0.01\text{ s}$  thus the CFL number of the cells - velocity times the time step divided by the cells spacing - is close to one. The shape of the filament is reported in Fig. 3.22 and 3.23. Fingering instabilities can be observed from the very beginning of the stretching, leading to branched structures, as described in [105, 5, 40]. Clearly, such complex shapes cannot be obtained using Lagrangian models, the mesh distortion would be too large.

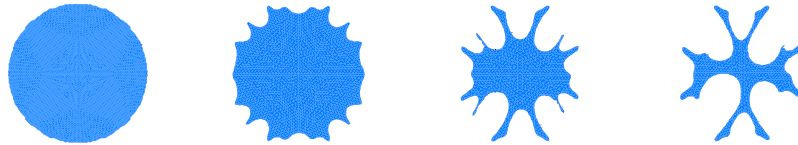


Figure 3.23: Filament stretching,  $\lambda = 0.421\text{ s}$  ( $We = 1.97$ ), aspect ratio  $L_0/R_0 = 1/20$ . Horizontal cut through the middle of the liquid region at time: (from left to right)  $t = 0\text{ s}$ ,  $t = 0.33\text{ s}$ ,  $t = 0.66\text{ s}$ ,  $t = 1\text{ s}$ .



# Bibliography

- [1] M. Aboubacar and M. F. Webster. Development of an optimal hybrid finite volume/element method for viscoelastic flows. *Internat. J. Numer. Methods Fluids*, 41(11):1147–1172, 2003.
- [2] E. Aulisa, S. Manservisi, and R. Scardovelli. A mixed markers and volume-of-fluid method for the reconstruction and advection of interfaces in two-phase and free-boundary flows. *J. Comput. Phys.*, 188(2):611–639, 2003.
- [3] F.P.T. Baaijens. Mixed finite element methods for viscoelastic flow analysis : a review. *J. Non Newtonian Fluid Mech.*, 79:361–385, 1998.
- [4] I. Babuška and A. K. Aziz. Survey lectures on the mathematical foundations of the finite element method. In *The mathematical foundations of the finite element method with applications to partial differential equations (Proc. Sympos., Univ. Maryland, Baltimore, Md., 1972)*, pages 1–359. Academic Press, New York, 1972. With the collaboration of G. Fix and R. B. Kellogg.
- [5] A. Bach, H.K. Rasmussen, P.-Y. Longin, and O. Hassager. Growth of non-axisymmetric disturbances of the free surface in the filament stretching rheometer: experiments and simulation. *J. Non Newtonian Fluid Mech.*, 108:163–186, 2002.
- [6] J. Baranger and D. Sandri. Finite element approximation of viscoelastic fluid flow: existence of approximate solutions and error bounds. I. Discontinuous constraints. *Numer. Math.*, 63(1):13–27, 1992.
- [7] J. Baranger and D. Sandri. A formulation of Stokes’s problem and the linear elasticity equations suggested by the Oldroyd model for viscoelastic flow. *RAIRO Modél. Math. Anal. Numér.*, 26(2):331–345, 1992.
- [8] J. Baranger and S. Wardi. Numerical analysis of a FEM for a transient viscoelastic flow. *Comput. Methods Appl. Mech. Engrg.*, 125(1-4):171–185, 1995.
- [9] J. W. Barrett, C. Schwab, and E. Süli. Existence of global weak solutions for some polymeric flow models. *Math. Models Methods Appl. Sci.*, 15(6):939–983, 2005.

- [10] J.W. Barrett and E. Süli. Existence of global weak solutions to some regularized kinetic models for dilute polymers. *Multiscale Model. Simul.*, 6(2):506–546 (electronic), 2007.
- [11] M. Bensaada and D. Esselaoui. Numerical analysis of stabilized method for transient viscoelastic flows. *Int. J. Pure Appl. Math.*, 21(4):441–473, 2005.
- [12] A.N. Beris, R.C. Armstrong, and R.A. Brown. Finite element calculation of viscoelastic flow in a journal bearing: I. small eccentricities. *J. Non-Newtonian Fluid Mech.*, 16(1-2):141–172, 1984.
- [13] R. Bird, C. Curtiss, R. Armstrong, and O. Hassager. *Dynamics of polymeric liquids, vol. 1 and 2*. John Wiley & Sons, New-York, 1987.
- [14] A. Bonito and E. Burman. A continuous interior penalty method for viscoelastic flows. *SIAM J. Sci. Comput.*, 30(3):1156–1177, 2008.
- [15] A. Bonito, Ph. Clément, and M. Picasso. Finite element analysis of a simplified stochastic Hookean dumbbells model arising from viscoelastic flows. *M2AN Math. Model. Numer. Anal.*, 40(4):785–814, 2006.
- [16] A. Bonito, Ph. Clément, and M. Picasso. Mathematical analysis of a simplified Hookean dumbbells model arising from viscoelastic flows. *J. Evol. Equ.*, 6(3):381–398, 2006.
- [17] A. Bonito, Ph. Clément, and M. Picasso. Mathematical and numerical analysis of a simplified time-dependent viscoelastic flow. *Numer. Math.*, 107(2):213–255, 2007.
- [18] A. Bonito, A. Lozinski, and Th. Mountford. Modeling viscoelastic flows using reflected stochastic differential equations. *Commun. Math. Sci.*, to appear.
- [19] A. Bonito, M. Picasso, and M. Laso. Numerical simulation of 3D viscoelastic flows with free surfaces. *J. Comput. Phys.*, 215(2):691–716, 2006.
- [20] J. Bonvin and M. Picasso. Variance reduction methods for connffessit-like simulations. *J. Non Newtonian Fluid Mech.*, 84:191–215, 1999.
- [21] J. Bonvin and M. Picasso. A finite element/Monte-Carlo method for polymer dilute solutions. *Comput. Vis. Sci.*, 4(2):93–98, 2001. Second AMIF International Conference (Il Ciocco, 2000).
- [22] J. Bonvin and M. Picasso. Mesoscopic models for viscoelastic flows: coupling finite element and Monte Carlo methods. *Monte Carlo Methods Appl.*, 8(1):73–81, 2002.
- [23] J. Bonvin, M. Picasso, and R. Stenberg. GLS and EVSS methods for a three-field Stokes problem arising from viscoelastic flows. *Comput. Methods Appl. Mech. Engrg.*, 190(29-30):3893–3914, 2001.

- [24] F. Brezzi. On the existence, uniqueness and approximation of saddle-point problems arising from Lagrangian multipliers. *Rev. Française Automat. Informat. Recherche Opérationnelle Sér. Rouge*, 8(R-2):129–151, 1974.
- [25] R.A. Brown, R.C. Armstrong, A.N. Beris, and P.W. Yeh. Galerkin finite element analysis of viscoelastic flows. *Comp. Meth. Appl. Mech. Engrg.*, 58:201–226, 1986.
- [26] A. Caboussat. Numerical simulation of two-phase free surface flows. *Archives of Computational Methods in Engineering, State of the art reviews*, 12(2):165–224, 2005.
- [27] A. Caboussat. A numerical method for the simulation of free surface flows with surface tension. *Comput. Fluids*, 35(10):1205–1216, 2006.
- [28] A. Caboussat, M. Picasso, and J. Rappaz. Numerical simulation of free surface incompressible liquid flows surrounded by compressible gas. *J. Comput. Phys.*, 203(2):626–649, 2005.
- [29] G. Caloz and J. Rappaz. Numerical analysis for nonlinear and bifurcation problems. In *Handbook of numerical analysis, Vol. V*, Handb. Numer. Anal., V, pages 487–637. North-Holland, Amsterdam, 1997.
- [30] C. Chauvière and A. Lozinski. An efficient technique for simulations of viscoelastic flows, derived from the Brownian configuration field method. *SIAM J. Sci. Comput.*, 24(5):1823–1837 (electronic), 2003.
- [31] C. Chauvière and R.G. Owens. How accurate is your solution?: Error indicators for viscoelastic flow calculations. *J. Non-Newtonian Fluid Mech.*, 95(1):1–33, 2000.
- [32] J.-Y. Chemin and N. Masmoudi. About lifespan of regular solutions of equations related to viscoelastic fluids. *SIAM J. Math. Anal.*, 33(1):84–112, 2001.
- [33] A. J. Chorin. Flame advection and propagation algorithms. *J. Comput. Phys.*, 35:1–11, 1980.
- [34] P. G. Ciarlet and J.-L. Lions, editors. *Handbook of numerical analysis. Vol. II*. Handbook of Numerical Analysis, II. North-Holland, Amsterdam, 1991. Finite element methods. Part 1.
- [35] J. Cormenzana, A. Ledd, M. Laso, and B. Debbaut. Calculation of free surface flows using CONNFFESSIT. *J. Rheology*, 45(1):237–258, 2001.
- [36] M.J. Crochet and R. Keunings. On numerical die swell calculation. *J. Non-Newtonian Fluid Mech.*, 10(1-2):85–94, 1982.
- [37] M.J. Crochet and K. Walters. Numerical methods in non-newtonian fluid mechanics. *Annual reviews of fluid mechanics*, 15:241–260, 1983.

- [38] P. Degond, M. Lemou, and M. Picasso. Viscoelastic fluid models derived from kinetic equations for polymers. *SIAM J. Appl. Math.*, 62(5):1501–1519, 2002.
- [39] P. Delaunay, A. Lozinski, and Owens R.G. Sparse tensor product Fokker-Planck based methods for nonlinear bead spring chain models of dilute polymer solutions. *CRM Proceedings & Lecture Notes*, 41:73–90, 2007.
- [40] D. Derk, A. Lindner, C. Creton, and D. Bonn. Cohesive failure of thin layers of soft model adhesives under tension. *J Appl. Phys.*, 93(3):1557–1566, 2003.
- [41] Q. Du, C. Liu, and P. Yu. FENE dumbbell model and its several linear and nonlinear closure approximations. *Multiscale Model. Simul.*, 4(3):709–731, 2005.
- [42] W. E, T. Li, and P. Zhang. Convergence of a stochastic method for the modeling of polymeric fluids. *Acta Math. Appl. Sin. Engl. Ser.*, 18(4):529–536, 2002.
- [43] W. E, T.J. Li, and P.W. Zhang. Well-posedness for the dumbbell model of polymeric fluids. *Comm. Math. Phys.*, 248(2):409–427, 2004.
- [44] V.J. Ervin and N. Heuer. Approximation of time-dependent, viscoelastic fluid flow: Crank-Nicolson, finite element approximation. *Numer. Methods Partial Differential Equations*, 20(2):248–283, 2004.
- [45] V.J. Ervin and J.S. Howell. A two-parameter defect-correction method for computation of steady-state viscoelastic fluid flow. *Appl. Math. Comp.*, 2008, to appear.
- [46] V.J. Ervin and W.W. Miles. Approximation of time-dependent viscoelastic fluid flow: SUPG approximation. *SIAM J. Numer. Anal.*, 41(2):457–486 (electronic), 2003.
- [47] V.J. Ervin and L.N. Ntasin. A posteriori error estimation and adaptive computation of viscoelastic fluid flow. *Numer. Methods Partial Differential Equations*, 21(2):297–322, 2005.
- [48] Y. Fan. Limiting behavior of the solutions of a falling sphere in a tube filled with viscoelastic fluids. *J. Non Newtonian Fluid Mech.*, 110(2-3):77–102, 2003.
- [49] K. Feigl, M. Laso, and H.C. Öttinger. The CONNFFESSIT approach for solving a two-dimensional viscoelastic fluid problem. *Macromolecules*, 28:3261–3274, 1995.
- [50] E. Fernández-Cara, F. Guillén, and R. R. Ortega. Mathematical modeling and analysis of viscoelastic fluids of the Oldroyd kind. In *Handbook of numerical analysis, Vol. VIII*, Handb. Numer. Anal., VIII, pages 543–661. North-Holland, Amsterdam, 2002.

- [51] N. Fiétier and M. Deville. Simulations of time-dependent flows of viscoelastic fluids with spectral element methods. *J. Sci. Comput.*, 17(1-4):649–657, 2002.
- [52] N. Fiétier and M.O. Deville. Simulations of time-dependent flows of viscoelastic fluids with spectral element methods. *J. Sci. Comput.*, 17(1-4):649–657, 2002.
- [53] A. Fortin, R. Guénette, and R. Pierre. On the discrete EVSS method. *Comput. Methods Appl. Mech. Engrg.*, 189(1):121–139, 2000.
- [54] M. Fortin and A. Fortin. A new approach for the fem simulation of viscoelastic flows. *J. Non-Newtonian Fluid Mech.*, 32(3):295–310, 1989.
- [55] M. Fortin and R. Pierre. On the convergence of the mixed method of Crochet and Marchal for viscoelastic flows. *Comput. Methods Appl. Mech. Engrg.*, 73(3):341–350, 1989.
- [56] L. Franca and S. Frey. Stabilized finite element methods. II. The incompressible Navier-Stokes equations. *Comput. Methods Appl. Mech. Engrg.*, 99(2-3):209–233, 1992.
- [57] V. Girault and P.-A. Raviart. *Finite element methods for Navier-Stokes equations*, volume 5 of *Springer Series in Computational Mathematics*. Springer-Verlag, Berlin, 1986. Theory and algorithms.
- [58] R. Glowinski. Finite element methods for incompressible viscous flow. In *Handbook of numerical analysis, Vol. IX*, Handb. Numer. Anal., IX, pages 3–1176. North-Holland, Amsterdam, 2003.
- [59] H.J.J. Gramberg, J.C. W. van Vroonhoven, and A.A.F. van de Ven. Flow patterns behind the free flow front for a Newtonian fluid injected between two infinite parallel plates. *Eur. J. Mech. B Fluids*, 23(4):571–585, 2004.
- [60] E. Grande, M. Laso, and M. Picasso. Calculation of variable-topology free surface flows using connffessit. *J. Non-Newtonian Fluid Mech.*, 113(2):127–145, 2003.
- [61] M. Griebel. Sparse grids and related approximation schemes for higher dimensional problems. In *Foundations of computational mathematics, Santander 2005*, volume 331 of *London Math. Soc. Lecture Note Ser.*, pages 106–161. Cambridge Univ. Press, Cambridge, 2006.
- [62] C. Guillopé and J.-C. Saut. Existence results for the flow of viscoelastic fluids with a differential constitutive law. *Nonlinear Anal.*, 15(9):849–869, 1990.
- [63] A. Hakim. Mathematical analysis of viscoelastic fluids of White-Metzner type. *J. Math. Anal. Appl.*, 185(3):675–705, 1994.

- [64] P. Halin, G. Lielens, R. Keunings, and V. Legat. The lagrangian particle method for macroscopic and micromacro viscoelastic flow computations. *J. Non-Newtonian Fluid Mech.*, 79(2-3):387–403, 1998.
- [65] D. Hu and T. Lelievre. New entropy estimates for the oldroyd-b model, and related models. *Comm. Math. Sci.*, 5(4):909–916, 2007.
- [66] M.A. Hulsen, R. Fattal, and R. Kupferman. Flow of viscoelastic fluids past a cylinder at high weissenberg number: Stabilized simulations using matrix logarithms. *J. Non-Newtonian Fluid Mech.*, 127(1):27–39, 2005.
- [67] M.A. Hulsen, A.P.G. van Heel, and B.H.A.A. van den Brule. Simulation of viscoelastic flows using brownian configuration fields. *J. Non-Newtonian Fluid Mech.*, 70:79–101, 1997.
- [68] H. Jin and R. I. Tanner. An a posteriori error estimate and adaptive refinement procedure for viscoelastic fluid flows: the modified upper-convected Maxwell model. *Comput. Mech.*, 13(6):400–413, 1994.
- [69] D. D. Joseph, M. Renardy, and J.-C. Saut. Hyperbolicity and change of type in the flow of viscoelastic fluids. *Arch. Rational Mech. Anal.*, 87(3):213–251, 1985.
- [70] B. Jourdain, C. Le Bris, T. Lelievre, and F. Otto. Long-time asymptotics of a multiscale model for polymeric fluid flows. *Arch. Rational Mech. Anal.*, 181(1):94–148, 2006.
- [71] B. Jourdain, T. Lelièvre, and C. Le Bris. Numerical analysis of micro-macro simulations of polymeric fluid flows: a simple case. *Math. Models Methods Appl. Sci.*, 12(9):1205–1243, 2002.
- [72] B. Jourdain, T. Lelièvre, and C. Le Bris. Existence of solution for a micro-macro model of polymeric fluid: the FENE model. *J. Funct. Anal.*, 209(1):162–193, 2004.
- [73] B. Jourdain, T. Lelièvre, and C. Le Bris. On a variance reduction technique for micromacro simulations of polymeric fluids. *J. Non Newtonian Fluid Mech.*, 122(1-3):91–106, 2004.
- [74] R. Keunings. On the high weissenberg number problem. *J. Non-Newtonian Fluid Mech.*, 20:209–226, 1986.
- [75] R. Keunings. Finite element methods for integral viscoelastic fluids. *Rheology Reviews*, pages 167–195, 2003.
- [76] R. Keunings. Micro-marco methods for the multi-scale simulation of viscoelastic flow using molecular models of kinetic theory. *Rheology Reviews*, pages 67–98, 2004.

- [77] J.M. Kim, C. Kim, J.H. Kim, C. Chung, K.H. Ahn, and S.J. Lee. High-resolution finite element simulation of 4:1 planar contraction flow of viscoelastic fluid. *J. Non-Newtonian Fluid Mech.*, 129(1):23–37, 2005.
- [78] P.E. Kloeden and E. Platen. *Numerical solution of stochastic differential equations*, volume 23 of *Applications of Mathematics (New York)*. Springer-Verlag, Berlin, 1992.
- [79] J. Koplik and J.R. Banavar. Extensional rupture of model non-newtonian fluid filaments. *Phys. Rev. E*, 67(011502), 2003.
- [80] A.P. Koppol, R. Sureshkumar, and B. Khomami. An efficient algorithm for multiscale flow simulation of dilute polymeric solutions using bead-spring chains. *J. Non-Newtonian Fluid Mech.*, 141(2-3):180–192, 2007.
- [81] M. Kröger. Simple models for complex nonequilibrium fluids. *Phys. Rep.*, 390(6):453–551, 2004.
- [82] R.G. Larson. *The Structure and Rheology of Complex Fluids*. Oxford University Press, Oxford, 1999.
- [83] M. Laso and H.-C. Öttinger. Calculation of viscoelastic flow using molecular models. *J. Non-Newtonian Fluid Mech.*, 47:1–20, 1993.
- [84] M. Laso, M. Picasso, and Öttinger H.C. 2d time-dependent viscoelastic flow calculations using CONNFFESSIT. *AICHE J.*, 43(4):877–892, 1997.
- [85] C. Le Bris and P.-L. Lions. Renormalized solutions of some transport equations with partially  $W^{1,1}$  velocities and applications. *Ann. Mat. Pura Appl. (4)*, 183(1):97–130, 2004.
- [86] Y.-J. Lee and J. Xu. New formulations, positivity preserving discretizations and stability analysis for non-Newtonian flow models. *Comput. Methods Appl. Mech. Engrg.*, 195(9-12):1180–1206, 2006.
- [87] T. Lelièvre. Optimal error estimate for the CONNFFESSIT approach in a simple case. *Comput. & Fluids*, 33(5-6):815–820, 2004.
- [88] P. Lesaint and P.-A. Raviart. On a finite element method for solving the neutron transport equation. In *Mathematical aspects of finite elements in partial differential equations (Proc. Sympos., Math. Res. Center, Univ. Wisconsin, Madison, Wis., 1974)*, pages 89–123. Publication No. 33. Math. Res. Center, Univ. of Wisconsin-Madison, Academic Press, New York, 1974.
- [89] T. Li, E. Vanden-Eijnden, P. Zhang, and W. E. Stochastic models of polymeric fluids at small deborah number. *J. Non Newtonian Fluid Mech.*, 121(2-3):117–125, 2004.

- [90] T. Li, H. Zhang, and P. Zhang. Local existence for the dumbbell model of polymeric fluids. *Comm. Partial Differential Equations*, 29(5-6):903–923, 2004.
- [91] T. Li and P. Zhang. Convergence analysis of BCF method for Hookean dumbbell model with finite difference scheme. *Multiscale Model. Simul.*, 5(1):205–234 (electronic), 2006.
- [92] A.E Likhtman and R.S. Graham. Simple constitutive equation for linear polymer melts derived from molecular theory: Roliepoly equation. *J. Non-Newtonian Fluid Mech.*, 114(1):1–12, 2003.
- [93] F. Lin, P. Zhang, and Z. Zhang. On the global existence of smooth solution to the 2-D FENE dumbbell model. *Comm. Math. Phys.*, 277(2):531–553, 2008.
- [94] F.H. Lin, C. Liu, and P. Zhang. On hydrodynamics of viscoelastic fluids. *Comm. Pure Appl. Math.*, 58(11):1437–1471, 2005.
- [95] P. L. Lions and N. Masmoudi. Global solutions for some Oldroyd models of non-Newtonian flows. *Chinese Ann. Math. Ser. B*, 21(2):131–146, 2000.
- [96] P.L. Lions and N. Masmoudi. Global existence of weak solutions to some micro-macro models. *C. R. Math. Acad. Sci. Paris*, 345(1):15–20, 2007.
- [97] C. Liu and N. J. Walkington. An Eulerian description of fluids containing visco-elastic particles. *Arch. Ration. Mech. Anal.*, 159(3):229–252, 2001.
- [98] A. Lozinski and C. Chauvière. A fast solver for Fokker-Planck equation applied to viscoelastic flows calculations: 2D FENE model. *J. Comput. Phys.*, 189(2):607–625, 2003.
- [99] A. Lozinski and R.G. Owens. An energy estimate for the Oldroyd B model: theory and applications. *J. Non-Newtonian Fluid Mech.*, 112:161–176, 2003.
- [100] A. Lunardi. *Analytic semigroups and optimal regularity in parabolic problems*. Progress in Nonlinear Differential Equations and their Applications, 16. Birkhäuser Verlag, Basel, 1995.
- [101] A. Machmoum and D. Esselaoui. Finite element approximation of viscoelastic fluid flow using characteristics method. *Comput. Methods Appl. Mech. Engrg.*, 190(42):5603–5618, 2001.
- [102] J. M. Marchal and M. J. Crochet. A new mixed finite element for calculating viscoelastic flow. *J. Non-Newtonian Fluid Mech.*, 28(1):77–114, 1987.
- [103] V. Maronnier, M. Picasso, and J. Rappaz. Numerical simulation of free surface flows. *J. Comput. Phys.*, 155(2):439–455, 1999.

- [104] V. Maronnier, M. Picasso, and J. Rappaz. Numerical simulation of 3d free surface flows. *Int. J. Numer. Methods Fluids*, 42(7):697–716, 2003.
- [105] G.H. McKinley and T. Sridhar. Filament-stretching rheometry of complex fluids. *Annu. Rev. Fluid Mech.*, 34:375–415, 2002.
- [106] M.A. Mendelson, P.W. Yeh, R.A. Brown, and R.C. Armstrong. Approximation error in finite element calculation of viscoelastic fluid flows. *J. Non-Newtonian Fluid Mech.*, 10(1-2):31–54, 1982.
- [107] G. Mompean and M. Deville. Unsteady finite volume simulation of oldroyd-b fluid through a three-dimensional planar contraction. *J. Non-Newtonian Fluid Mech.*, 72(2-3):253–279, 2000.
- [108] K. Najib and D. Sandri. On a decoupled algorithm for solving a finite element problem for the approximation of viscoelastic fluid flow. *Numer. Math.*, 72(2):223–238, 1995.
- [109] K. Najib, D. Sandri, and A.-M. Zine. On a posteriori estimates for a linearized Oldroyd’s problem. *J. Comput. Appl. Math.*, 167(2):345–361, 2004.
- [110] W. F. Noh and P. Woodward. *SLIC (Simple Line Interface Calculation)*, volume 59 of *Lectures Notes in Physics*, pages 330–340. Springer-Verlag, 1976.
- [111] A. Novotný, A. Sequeira, and J.H. Videman. Steady motions of viscoelastic fluids in three-dimensional exterior domains. Existence, uniqueness and asymptotic behaviour. *Arch. Ration. Mech. Anal.*, 149(1):49–67, 1999.
- [112] S. Osher and R. Fedkiw. *Level set methods and dynamic implicit surfaces*, volume 153 of *Applied Mathematical Sciences*. Springer-Verlag, New York, 2003.
- [113] H.-C. Öttinger. *Stochastic processes in polymeric fluids*. Springer-Verlag, Berlin, 1996.
- [114] H.-C. Öttinger, B.H.A.A. van den Brule, and M.A. Hulsen. Brownian configuration fields and variance reduced CONNFFESSIT. *J. Non-Newtonian Fluid Mech.*, 70:255–261, 1997.
- [115] R.G. Owens. A posteriori error estimates for spectral element solutions to viscoelastic flow problems. *Comput. Methods Appl. Mech. Engrg.*, 164(3-4):375–395, 1998.
- [116] M. Picasso and J. Rappaz. Existence, a priori and a posteriori error estimates for a nonlinear three-field problem arising from Oldroyd-B viscoelastic flows. *M2AN Math. Model. Numer. Anal.*, 35(5):879–897, 2001.

- [117] E. Picheli and T. Coupez. Finite element solution of the 3D mold filling problem for viscous incompressible fluid. *Comput. Methods Appl. Mech. Engrg.*, 163(1-4):359–371, 1998.
- [118] O. Pironneau. *Finite Element Methods for Fluids*. Wiley, Chichester, 1989.
- [119] O. Pironneau, J. Liou, and T. Tezduyar. Characteristic-Galerkin and Galerkin/least-squares space-time formulations for the advection-diffusion equation with time-dependent domains. *Comp. Meth. Appl. Mech. Eng.*, 100:117–141, 1992.
- [120] A. Quarteroni and A. Valli. *Numerical Approximation of Partial Differential Equations*. Number 23 in Springer Series in Computational Mathematics. Springer-Verlag, 1991.
- [121] H.K. Rasmussen and O. Hassager. Three-dimensional simulations of viscoelastic instability in polymeric filaments. *J. Non Newtonian Fluid Mech.*, 82:189–202, 1999.
- [122] M. Renardy. Existence of slow steady flows of viscoelastic fluids with differential constitutive equations. *Z. Angew. Math. Mech.*, 65(9):449–451, 1985.
- [123] M. Renardy. A local existence and uniqueness theorem for a K-BKZ-fluid. *Arch. Rational Mech. Anal.*, 88(1):83–94, 1985.
- [124] M. Renardy. An existence theorem for model equations resulting from kinetic theories of polymer solutions. *SIAM J. Math. Anal.*, 22(2):313–327, 1991.
- [125] M. Renardy. *Mathematical analysis of viscoelastic flows*, volume 73 of *CBMS-NSF Regional Conference Series in Applied Mathematics*. Society for Industrial and Applied Mathematics (SIAM), Philadelphia, PA, 2000.
- [126] D. Revuz and M. Yor. *Continuous martingales and Brownian motion*, volume 293 of *Grundlehren der Mathematischen Wissenschaften [Fundamental Principles of Mathematical Sciences]*. Springer-Verlag, Berlin, 1994.
- [127] W.J. Rider and D.B. Kothe. Reconstructing volume tracking. *J. Comput. Phys.*, 141(2):112–152, 1998.
- [128] V. Ruas, J. H. Carneiro de Araújo, and M. A. M. Silva Ramos. Approximation of the three-field Stokes system via optimized quadrilateral finite elements. *RAIRO Modél. Math. Anal. Numér.*, 27(1):107–127, 1993.
- [129] D. Sandri. Analyse d’une formulation à trois champs du problème de Stokes. *RAIRO Modél. Math. Anal. Numér.*, 27(7):817–841, 1993.

- [130] D. Sandri. Finite element approximation of viscoelastic fluid flow: existence of approximate solutions and error bounds. Continuous approximation of the stress. *SIAM J. Numer. Anal.*, 31(2):362–377, 1994.
- [131] D. Sandri. Non-integrable extra stress tensor solution for a flow in a bounded domain of an Oldroyd fluid. *Acta Mech.*, 135(1-2):95–99, 1999.
- [132] D. Sandri. Numerical study around the corotational Maxwell model for the viscoelastic fluid flows. *Eur. J. Mech. B Fluids*, 24(6):733–750, 2005.
- [133] P. Saramito. A new  $\theta$ -scheme algorithm and incompressible FEM for viscoelastic fluid flows. *RAIRO Modél. Math. Anal. Numér.*, 28(1):1–35, 1994.
- [134] R. Scardovelli and S. Zaleski. Direct numerical simulation of free-surface and interfacial flow. In *Annual review of fluid mechanics, Vol. 31*, volume 31 of *Annu. Rev. Fluid Mech.*, pages 567–603. Annual Reviews, Palo Alto, CA, 1999.
- [135] C. Schwab and M. Suri. Mixed  $hp$  finite element methods for Stokes and non-Newtonian flow. *Comput. Methods Appl. Mech. Engrg.*, 175(3-4):217–241, 1999.
- [136] J. A. Sethian and P. Smereka. Level set methods for fluid interfaces. In *Annual review of fluid mechanics, Vol. 35*, volume 35 of *Annu. Rev. Fluid Mech.*, pages 341–372. Annual Reviews, Palo Alto, CA, 2003.
- [137] P. Singh, D.D. Joseph, T. I. Heslab, R. Glowinski, and T.-W. Pan. A distributed lagrange multiplier/fictitious domain method for viscoelastic particulate flows. *J. Non Newtonian Fluid Mech.*, 91(2-3):165–188, 2000.
- [138] M.F. Tomé, Castelo A., and J.A. Cuminato. A numerical method for solving the Oldroyd-B model for 3d free surface flows. *J. Non Newtonian Fluid Mech.*, 2008.
- [139] M.F. Tomé, N. Mangiavacchi, J.A. Cuminato, A. Castelo, and S. McKee. A finite difference technique for simulation unsteady viscoelastic free surface flows. *J. Non Newtonian Fluid Mech.*, 106:61–106, 2002.
- [140] M.F. Tomé and S. McKee. Numerical simulation of viscous flow: buckling of planar jets. *Int. J. Numer. Meth. Fluids.*, 29:705–718, 1999.
- [141] A. Trebotich, P. Colella, and G.H. Miller. A stable and convergent scheme for viscoelastic flow in contraction channels. *J. Comput. Phys.*, 205:315–342, 2005.
- [142] W.M.H. Verbeeten, G.W.M. Peters, and Baaijens F.P.T. Numerical simulations of the planar contraction flow for a polyethylene melt using the xpp model. *J. Non-Newtonian Fluid Mech.*, 117(2-3):73–84, 2004.

- [143] T. von Petersdorff and C. Schwab. Numerical solution of parabolic equations in high dimensions. *M2AN Math. Model. Numer. Anal.*, 38(1):93–127, 2004.
- [144] P. Wapperom and M. Renardy. Numerical prediction of the boundary layers in the flow around a cylinder using a fixed velocity field. *J. Non-Newtonian Fluid Mech.*, 125(1):35–48, 2005.
- [145] M. Yao and G.H. McKinley. Numerical simulation of extensional deformations of viscoelastic liquid bridges in filament stretching devices. *J. Non-Newtonian Fluid Mech.*, 74(1-3):47–88, 1998.
- [146] H. Zhang and P. Zhang. Local existence for the FENE-Dumbbells model of polymeric liquids. *Arch. Rational Mech. Anal.*, 181:373–400, 2006.
- [147] L.Y. Zhang, H. Zhang, and P.W. Zhang. Global existence of weak solutions to the regularized hookean dumbbell model. *Commun. Math. Sci.*, 6(1):85–124, 2008.

# Index

- CFL number, 46, 55, 57, 60, 62, 63
- characteristics, method of, 29, 45, 46
- constitutive equation, *see* models
- convergence, 15, 19–21, 24, 25, 27, 30, 36, 37, 39, 43, 46, 57, 59
- Deborah number, *see* time relaxation
- existence, 19, 22–25, 27, 31, 36, 37, 39, 40, 43
- extra-stress, 7–10, 13–17, 20, 21, 23–25, 28–30, 33, 34, 37, 46, 50, 52–57
- filament stretching, 6, 16, 51, 55, 60, 62, 63
- fingering instabilities, 7, 62
- finite elements, *see* Galerkin
- free surface, 5, 15–17, 19, 28, 30, 36, 39, 45, 54, 55, 57, 58
- Galerkin, 27, 33, 36, 45, 46, 52
  - finite elements, 19
  - stabilization, 21, 34, 36–38, 40, 41, 52, 53
  - EVSS, 20, 35, 36, 52, 54
  - GLS, 20, 34, 36
- inf-sup condition, 20, 24, 31–34, 36
- jet buckling, 7, 55, 59, 61
- level set, 7
- models
  - differential, 8
  - Extended Pom-Pom, 9
  - FENE, 10, 12–14, 17, 21, 23–25, 28, 30, 36, 54
- FENE-P, 14
- Fokker-Planck, 13, 14, 21, 24
- Giesekus, 9, 23
- Hookean, 13
- Hookean dumbbells, 9, 13, 14, 19, 23–27, 30, 39
- integral, 8–10, 23
- Jeffreys, 23
- K-BKZ, 10, 23
- Leonov, 9
- Maxwell
  - corotational, 21
  - upper convected, 8, 20, 22, 23
- Oldroyd-B, 8–10, 14, 16, 17, 19, 20, 22–25, 28, 29, 36, 45, 52, 53, 55, 60
  - corotational, 8, 23
- Phan-Thien Tanner, 9, 23
- reflected dumbbells, 13
- Rolie-Poly, 9
- Rouse chain, 10, 11, 14
- Monte-Carlo, 15, 26, 27, 39
- operator splitting, 19, 27, 28, 45
- polymer, 5–13, 21, 22, 37
- SLIC, 46, 48, 49
- solvent, 6–8, 10, 11, 23, 31, 37
- stochastic, 11–16, 21, 23, 24, 39, 41
- Stokes, 19, 20, 24, 25, 31, 35, 36, 38, 52, 53, 62
- time relaxation, 8, 10, 12, 14, 20–23, 37, 60
- VOF, 28, 30, 46–52, 54, 56

Weissenberg number, *see* time relaxation